I.O.S.

AN INSTRUMENT TO MEASURE DIFFERENTIAL PORE PRESSURES IN DEEP OCEAN SEDIMENTS: POP–UP–PORE–PRESSURE–INSTRUMENT (PUPPI)

BY

P. J. SCHULTHEISS, S. D. McPHAIL,

A. R. PACKWOOD AND B. HART

REPORT NO. 202

1985

OCEAN DISPOSAL OF HIGH LEVEL RADIOACTIVE WASTE
A RESEARCH REPORT PREPARED FOR THE DEPARTMENT
OF THE ENVIRONMENT

NATURAL ENVIRONMENT RESEARCH COUNCIL

INSTITUTE OF OCEANOGRAPHIC SCIENCES

INSTITUTE OF OCEANOGRAPHIC SCIENCES

Wormley, Godalming,
Surrey, GU8 5UB.
(0428 - 79 - 4141)

(Director: Dr. A.S. Laughton FRS)

Bidston Observatory,
Birkenhead,
Merseyside, L43 7RA.
(051 - 653 - 8633)

(Assistant Director: Dr D.E. Cartwright FRS)

Crossway,
Taunton,
Somerset, TA1 2DW.
(0823 - 86211)

(Assistant Director: M.J. Tucker)

When citing this document in a bibliography the reference should be given as follows:-

SCHULTHEISS, P.J., McPHAIL, S.D., PACKWOOD, A.R. & HART, B. 1985 An instrument to measure differential pore pressures in deep ocean sediments: Pop-Up-Pore-Pressure-Instrument (PUPPI). *Institute of Oceanographic Sciences, Report*, No. 202, 57pp.

INSTITUTE OF OCEANOGRAPHIC SCIENCES

WORMLEY

An instrument to measure differential pore pressures in deep ocean sediments: Pop-Up-Pore-Pressure-Instrument (PUPPI)

by

P.J. Schultheiss, S.D. McPhail,
A.R. Packwood and B. Hart

I.O.S. Report No. 202

1985

DEPARTMENT OF THE ENVIRONMENT
RADIOACTIVE WASTE MANAGEMENT
RESEARCH PROGRAMME 1982/84

DoE Report No.: DoE/RW/84/165

Contract Title: DoE selection and evaluation of sites for the disposal of high-level radioactive waste.

DoE Reference: DGR 481/179

Report Title: An instrument to measure differential pore pressures in deep ocean sediments: Pop-Up-Pore-Pressure Instrument (PUPPI)

Authors: SCHULTHEISS, P.J., McPHAIL, S.D., PACKWOOD, A.R. and HART, B.

Date of submission to DoE: 5 September 1984

Period covered by report: June 1980 to November 1983

ABSTRACT

A Pop-Up-Pore-Pressure-Instrument (PUPPI) has been developed to measure differential pore pressures in sediments. The differential pressure is the pressure above or below normal hydrostatic pressure at the depth of the measurement. It is designed to operate in water depths up to 6000 metres for periods of weeks or months, if required, and measures differential pore pressures at depths of up to 3 metres into the sediments with a resolution of 0.05 kPa. It is a free-fall device with a lance which penetrates the sediments. This lance and the ballast weight is disposed when the PUPPI is acoustically released from the sea floor. When combined with permeability and porosity values of deep-sea sediments the pore pressure measurements made using the PUPPI suggest advection velocities as low as 8.8 mm/yr. The mechanical, electrical and acoustic systems are described together with data obtained from both shallow and deep water trials.

Keywords:
299
Disposal under deep ocean bed (94)
Hydrogeology (111)
Geotechnics (113)
Sediment structure/permeability (117)
Field experiments (124)

This work has been commissioned by the Department of the Environment as part of its radioactive waste management research programme. The results will be used in the formulation of Government policy but, at this stage, they do not necessarily represent Government policy.

CONTENTS

LIST OF FIGURES

1. INTRODUCTION

The impetus for the development of an instrument to measure pore pressures in sediments stems from the wide-ranging study into the feasibility of disposing of high-level radioactive waste in deep ocean sediments. It is considered that the burial of these wastes into oceanic sediments may provide a series of barriers that would isolate man from the long-lived radionuclides (Hinga et al., 1982). The barriers consist of the wasteform itself (probably vitrified), the container, the sediments and the ocean waters. While it is conceivable that the wasteform and canister may provide adequate containment, possibly for a few hundred years, the primary barrier must be considered to be the sediments which, for many thousands of years, must impede the migration of radionuclides until their activity decays to a safe level. Possible transport mechanisms within deep sea sediments are, therefore, of considerable importance to the overall model which will predict the leak rate of hazardous isotopes into the ocean waters.

Migration of radionuclides in water-saturated, porous sediments from a given source will be driven by diffusion and pore-water advection. Both these processes will be modified by the adsorption characteristics which will depend on the complex geochemistry of the sediments. It is the pore water advection parameter which is addressed in this report because the measurement of pore pressure is one of three parameters that are needed to quantify the advection.

Evidence for the existence of pore water advection comes mainly from measurements of non-linear temperature profiles within the sediments. It is generally accepted that anomalously-low measured values of conductive heat flux in areas close to active spreading centres can be accounted for by hydrothermal circulation through the highly-permeable ocean crust (Noel, 1983). Direct observations of hydrothermal circulation in young oceanic crust (Corliss et al., 1979; RISE, 1980; Macdonald & Luyendyk, 1981; Anderson et al., 1982) provide further evidence for this process. As the ocean crust ages and moves away from active spreading centres, it cools, becomes less permeable (hydrothermal minerals precipitate in the fractures) and is overlain with a blanket of sediments with low permeabilities. Consequently, a change in the hydrothermal convection occurs whereby, eventually, any remaining convection is confined to the basement, and heat flow through the sediments occurs by conduction only. This change in pattern is shown schematically in Figure 1. The oscillatory pattern has been predicted from closely-spaced measurements of heat flow (see Noel, 1983). The transition zone, where convection occurs through the sediments, has been inferred

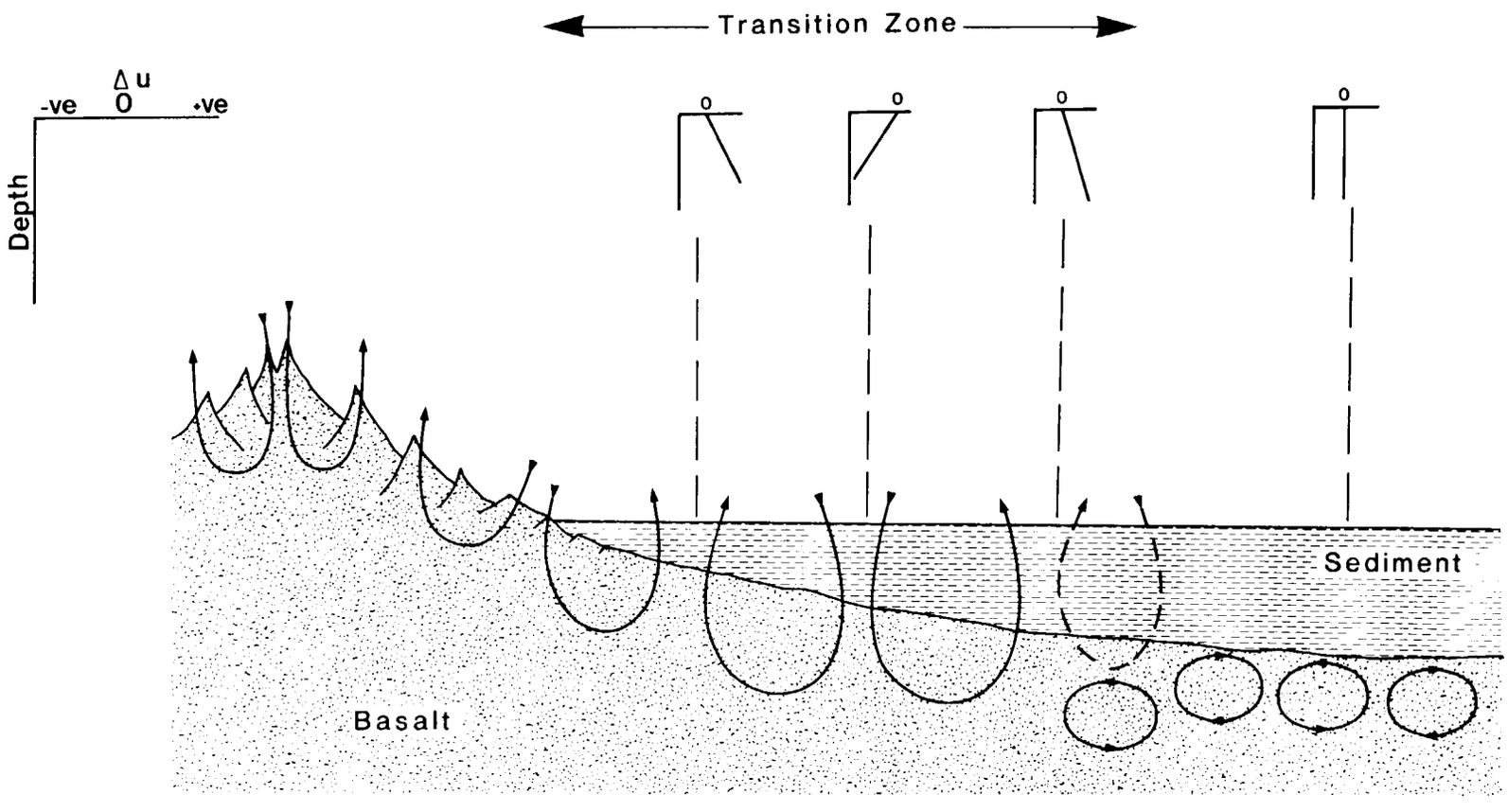

Figure 1: Schematic section through ocean spreading centre and ageing ocean crust showing the possible changes in hydrothermal circulation caused by overlying sediments and reduction in basalt permeability. Graphs predict the nature of the differential pore pressure profiles (after Noel, 1983).

from non-linear temperature profiles. The non-linearity of temperature profiles has been used as evidence of this type of pore-water advection through sediments in the Crozet and Madagascar Basins (Anderson et al., 1979), the Sohm Abyssal Plain (Burgess & Judge, 1981), the Brazil Basin (Langseth & Herman, 1981), the Galapagos Rift (Becker & Von Herzen, 1983; Williams et al., 1979) and the Mariana Trough (Abbott et al., 1983). In these reports, the advection velocities estimated from non-linear temperature profiles, using techniques described by Noel (1983), are typically 1 m y^{-1}.

Noel (1983) discusses temperature profiles obtained from ten sites in the North East Atlantic, three of which had significantly non-linear profiles. One interpretation of these profiles yields calculated advection velocities of 0.52, 1.12 and 6 m y^{-1}.

Crowe and McDuff (1979) have compared pore-water advection velocities calculated from both temperature profiles and pore-water chemistry (assuming zero diffusion) from three sites in the equatorial Pacific. It was found that the velocities calculated using sulphate diffusion-convection-reaction models were 2-3 orders of magnitude lower than velocities calculated from the non-linear temperature profiles. This inconsistency led Noel (1983a) to consider mechanisms, other than advection, which might give rise to the now widely-reported, non-linear temperature profiles. He concluded that several other mechanisms could be responsible including: sediment disturbance (caused by the entry of the probe), bottom-water temperature changes of only a few hundredths of a degree and modest topographic relief. Consequently, while the geothermal measurements and direct observations indicate that hydrothermal convection does exist (especially at active spreading centres), there is considerable doubt about the ability of temperature profiles to provide accurate measurements of pore water advection rates in sediments. In view of the importance of this topic to the feasibility of high-level radioactive waste disposal another technique, which involves directly measuring the pore pressures in sediments, has been pursued and is the subject of this report.

2. PORE WATER FLUXES

Any flux of water through a porous medium will be accompanied by a pressure gradient. The relationship which relates pore pressure to volume flow was found empirically by Darcy and can be simply expressed as

$$Q = kAi \qquad (1)$$

where Q is the rate of flow (m^3/s)

k is the permeability (m/s)

A is the cross-sectional area (m^2)

i is the hydraulic gradient = h/l

The hydraulic gradient, i, is the ratio of the pressure difference across the sample (expressed as a height of water, h) and the thickness of the porous sample, l (see Figure 2). The velocity of an element of water approaching the porous layer, V_a (approach velocity), is given by

$$V_a = Q/A = ki \tag{2}$$

and the velocity of an element of water in the porous layer, V (seepage velocity) is given by

$$V = \frac{V_a}{n} = \frac{ki}{n}$$

where n is the porosity of the porous layer.

It is readily apparent that this simple expression given by (3) could be used to determine the velocity of an element of water moving in deep-sea sediments.

Consider a model consisting of three sedimentary layers with vertical permeabilities and thicknesses: k_1, z_1; k_2, z_2; k_3, z_3. Assume that the pore water is moving vertically upwards with an unknown volumetric flow rate, Q, and that the total differential pore pressure across the three layers is ΔU_T (expressed as a height of water). Therefore, from Darcy's law, for a unit cross-sectional area,

$$Q = k_1 i_1 = k_2 i_2 = k_3 i_3$$

hence
$$Q = \frac{k_1 \Delta U_1}{z_1} = \frac{k_2 \Delta U_2}{z_2} = \frac{k_3 \Delta U_3}{z_3} \tag{4}$$

and
$$\Delta U_T = \Delta U_1 + \Delta U_2 + \Delta U_3 \tag{5}$$

where ΔU_1, 2, 3 is the differential pore pressure across layers 1, 2 and 3

from (4)
$$\Delta U_2 = \frac{k_1 z_2}{k_2 z_1} \Delta U_1 \text{ and } \Delta U_3 = \frac{k_1 z_3}{k_3 z_1} \Delta U_1 \tag{6}$$

from (5) and (6)
$$\Delta U_1 = \frac{\Delta U_T}{1 + \frac{k_1}{z_1}\left(\frac{z_2}{k_2} + \frac{z_3}{k_3}\right)} \tag{7}$$

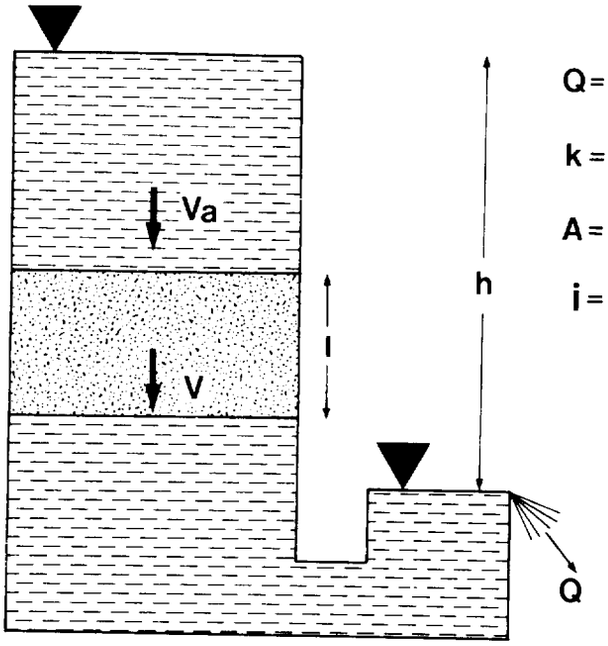

Q= flow rate ($m^3 s^{-1}$)

k= permeability ($m s^{-1}$)

A= cross sectional area (m^2)

i= hydraulic gradient (h/l)

Darcy's Law $Q = \frac{kAh}{l}$

Approach Velocity $V_a = ki$

Seepage Velocity $V = \frac{ki}{n}$

Figure 2: Schematic diagram of flow through porous media governed by Darcy's Law.

Values of ΔU_2 and ΔU_3 can then be obtained from equation 4. The velocity of an element of water in a layer is given by equation 3

$$V = \frac{ki}{n} = \frac{k\Delta U}{nz} \tag{8}$$

where the hydraulic gradient $i = \Delta U/z$

therefore the time taken for an element to move through a layer, t, is given by

$$t = \frac{nz^2}{k\Delta U} \tag{9}$$

The total time for an element of water to migrate through all three layers, T, is given by

$$T = t_1 + t_2 + t_3$$

It is clear that the above argument could be applied to any number of different layers, m, to any depth. Therefore:

$$T = \sum_{j=1}^{j=m} n_j z_j^2 / k_j \Delta U_j \tag{10}$$

Furthermore, (10) shows that to calculate T we must know the permeability, thickness and porosity of each layer but from (7) we need to know only the excess pore pressure at one point anywhere in the section.

Consequently, a programme of research began at IOS to measure pore-water velocities and, in particular, T from the four parameters in equation 10.

Porosity (n), depth (z) and permeability (k) can all be measured from core samples, although core size and disturbance will limit the accuracy to which the measurements can be made. Permeability is the most difficult to measure accurately in the laboratory and is the subject of another report (Schultheiss, 1984). The differential pore pressure (ΔU_T) is the only parameter that cannot be measured in the laboratory and must be measured in situ. The total differential pore pressure at any point in the sediment is defined as the pressure difference between the actual pressure and the hydrostatic pressure at that point. ΔU can be positive, leading to an upward flow of water, or negative, leading to a downward flow of water. The term "excess pore pressure" is often used to denote ΔU_T but the term is not strictly correct when dealing with negative differential pressures.

The complete programme to measure pore-water advection is shown in a flow chart (Figure 3). This report deals exclusively with the first box (design and build pop-up-pore-pressure instrument, PUPPI).

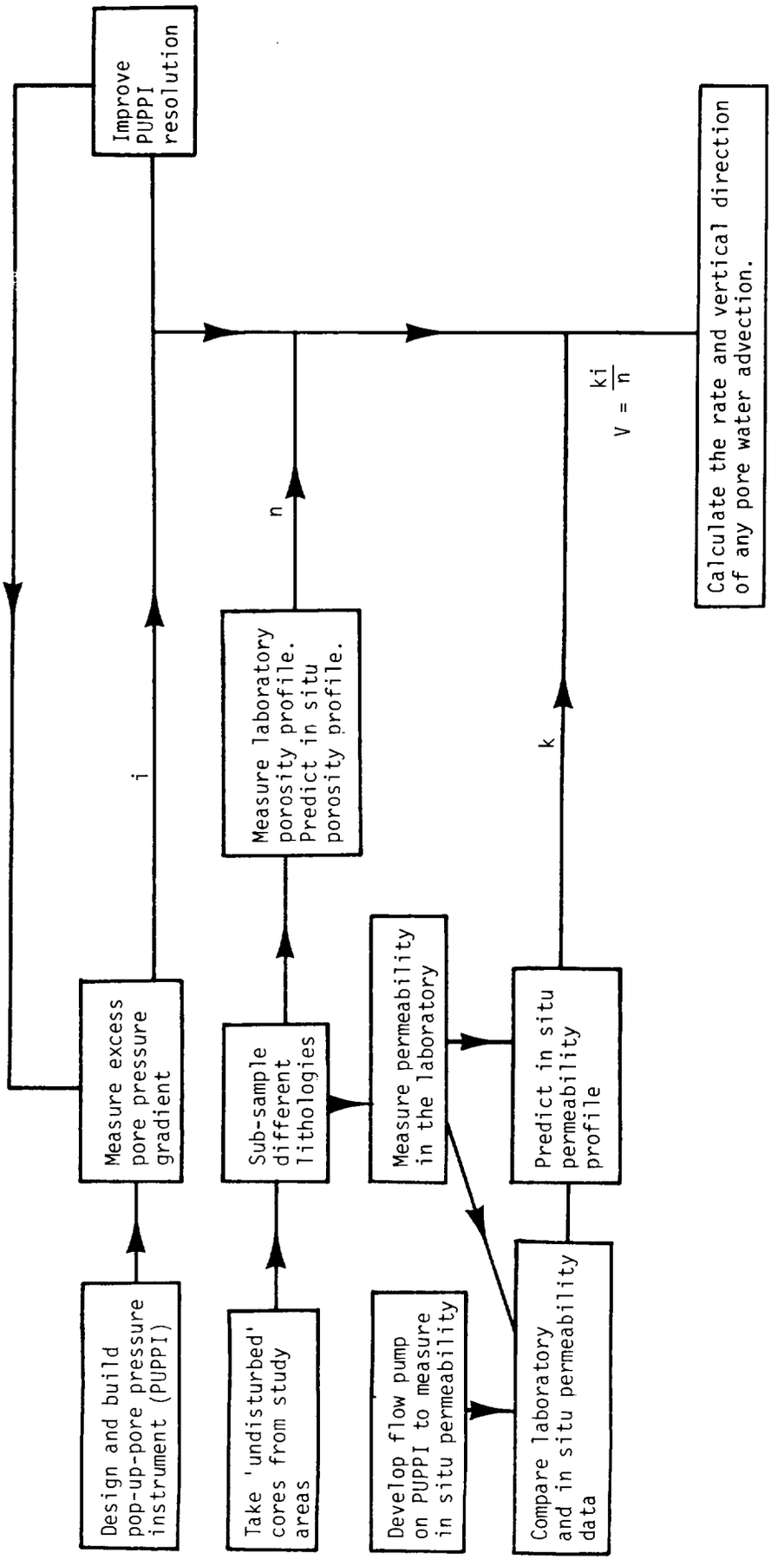

Figure 3: Flow chart of IOS programme to measure pore water fluxes in deep sea sediments.

3. DESIGN CONSIDERATIONS

The first and primary requirement of the instrument is that it should accurately measure the differential pore pressure (ΔU) at some depth (z) in the sediment. The accuracy to which the pore pressure needs to be measured is the first to be examined. Klett (1983) has used a computer model to investigate the the effects of natural pore water advection on the release of radionuclides buried at depths of up to 40 m. Several conclusions were reached which are worth repeating.

"Pore water velocities less than 0.1 mm/yr have no effect on isotopic release to the ocean."

"In the velocity range from 0.1 mm/yr to 1 cm/year the presence of natural pore water convection increases isotopic release. Release can be reduced by increasing burial depth. However, the slopes of the release/velocity curves are large in this region and a small change or error in velocity would cause a large change in release."

"If velocities are greater than 1 cm/yr, increasing burial depth to 40m will not reduce the release fraction to acceptable levels."

With a velocity of 0.1 mm/yr it would take an element of water 300,000 years to reach the surface if buried at 30m. It seems reasonable, therefore, to have initially a target resolution of the instrument which is capable of resolving advection velocities down to 0.1 mm/yr.

If we consider a homogeneous, isotropic sediment in which there is an advection velocity, V, then the relationship between the differential pore pressure ΔU (expressed as a head of water, m) and V is given by equation 8. Let z equal 3m (which is a reasonable length for a probe) and n = 0.666 then this equation becomes

$$V = k\Delta U/20 \ ms^{-1} \qquad (11)$$

Figure 4 illustrates this simple relationship between V and ΔU as a nomogram for sediments of different permeabilities. It can be seen that because the range of interest of k and V covers several orders of magnitude, so does ΔU. For a pelagic clay (where $k = 10^{-7}$ mm/s), ΔU at 3m, with an advection velocity of 0.1 mm/y, is approximately 0.7 kPa whereas for a silt ($k = 10^{-3}$ mm/s), ΔU is less than 10^{-4} kPa. However, for advection velocities of 1 m/yr (as indicated by some non-linear temperature profiles) ΔU would be 7000 kPa and 0.7 kPa for a clay and a silt respectively.

Positive pore pressures as high as 7000 kPa cannot exist in sediments because of the following reasoning. The shear strength of a water-saturated

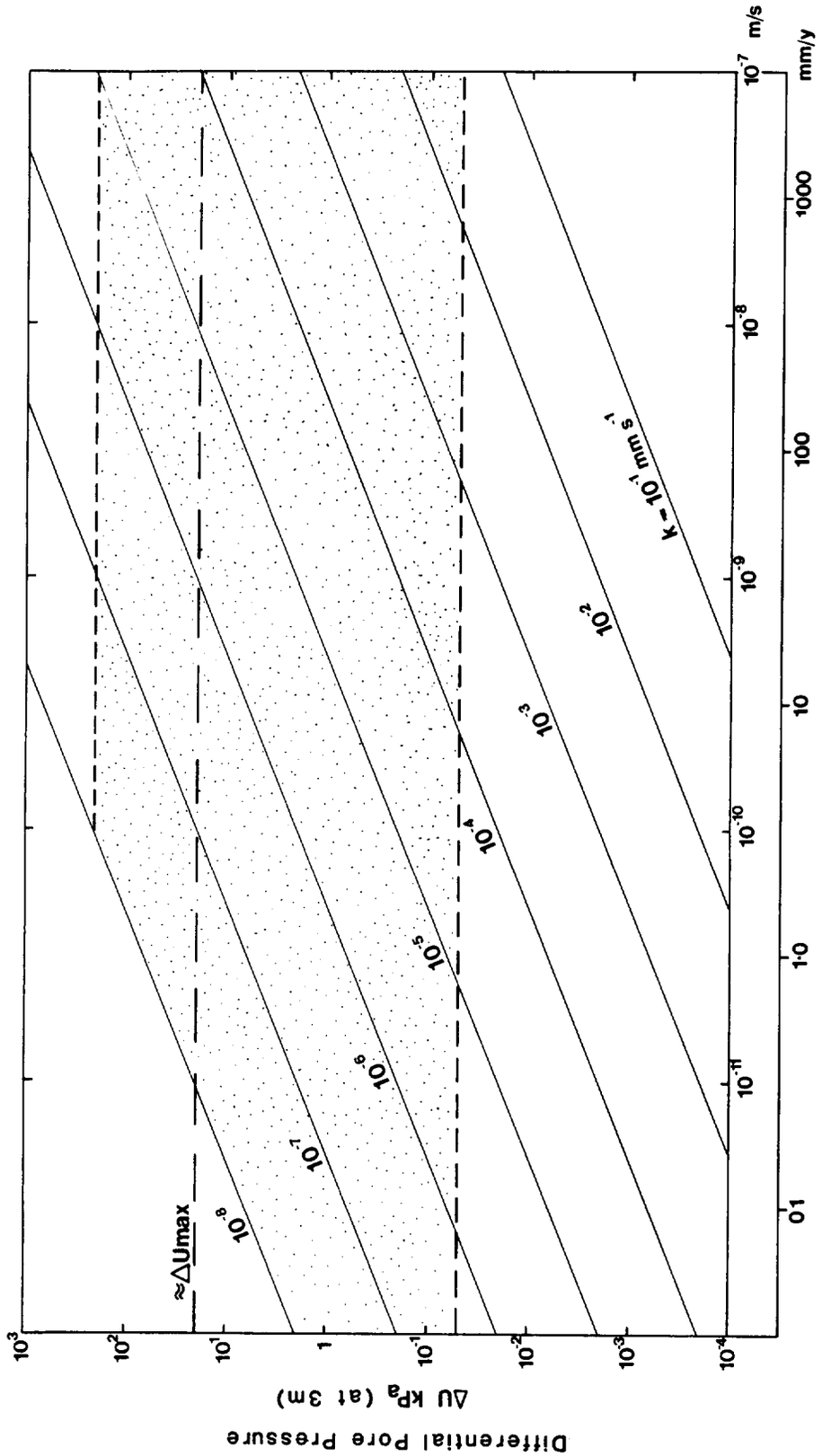

Figure 4: Nomogram for determining the advection velocity from the differential pore pressure and the permeability, k, for different sediments. u is calculated at 3 metres assuming the sediment is isotropic and has a porosity of 0.67. The stippled area indicates the pressure range of the transducers, and u_{max} is the estimated maximum +ve pore pressure.

sediment may be expressed by the Mohr-Coulomb relationship:

$$s = \bar{c} + \bar{\sigma} \tan \bar{\phi} \qquad (12)$$

where $\bar{c}$ = cohesion

$\bar{\phi}$ = effective angle of internal friction

$\bar{\sigma}$ = effective normal stress

$$\bar{\sigma} = \sigma - u \qquad (13)$$

where σ = total normal stress

u = pore water pressure

For a sediment with a known density profile, σ can be obtained for any depth by integrating the submerged unit weights. Typically, at a depth of 3m, σ will be about 12 kPa, therefore, any pore pressures greater than this value will create negative effective stresses. The shear strength in cohesionless sediments (silts and sands) will, under this condition, be zero and they will exhibit fluid-like properties. For clays, the cohesion parameter may be a few kPa, therefore, even in clays it is improbable that steady state pore pressures at 3m can be greater than about 20 kPa. This value is shown as ΔU_{max} in Figure 4. The implication of this is, for example, that in a sediment with $k = 10^{-7}$ mm/s the maximum upward pore-water advection velocity is 10^{-10} m/s ($\simeq$3 mm/y) (intercept of ΔU_{max} and $k = 10^{-7}$). It should be noted that there is no corresponding maximum for downward advection velocity. Obviously, the above analysis is totally incompatible with estimates of any upward pore-water advection velocities of greater than only a few centimetres per year. A differential pressure transducer was chosen that would have a range of up to 200 kPa with a resolution, (combined with the electronics and data logger) of around 0.05 kPa. This range, which is shown by the stippled area in Figure 4, is possibly one or two orders of magnitude short of the desired resolution for coarser sediments but covers the major range of interest.

One of the difficulties in measuring in-situ pore pressures is the problem of disturbance. When a probe enters the sediment the pore pressure will initially increase because of the sediment displacement. This pressure pulse will decay with time at a rate depending on a multitude of factors including primarily the permeability and consolidation parameters of the sediment. For clays it may take several days for the pore pressure to become constant. Consequently, a tethered instrument was considered impractical. The original concept was to employ a three-stage device consisting of: (a) driving force

(lead weights), (b) buoyant instrumentation and data logger, and (c) a lance to penetrate 3m into the sediment. With this configuration, the instrument would be lowered into the sea bed on the ship's warp, information regarding angle and depth of penetration being acoustically telemetered to the ship. If satisfactory, the lead weights and warp would be released from the instrument and hauled in, leaving the instrument undisturbed on the seafloor for up to several days. Unsatisfactory entry would be followed by withdrawing the device and re-entering until full penetration and no tilt was recorded. Recovery would consist of acoustically releasing the buoyant package leaving the disposable lance behind. This was the concept of PUPPI Mark I (Pop-Up-Pore-Pressure-Instrument).

It transpired, however, that, despite the advantages of its versatility, the strain imposed on the mechanical release mechanism, caused by severe oscillations on the warp, was enough to pre-trigger the device. PUPPI Mark I was lost during a wire test on Discovery Cruise 131.

It was decided to simplify this concept and build a free-fall device which would dispose of both the lance and the lead weights on recovery.

4. MECHANICAL DESIGN ASPECTS

The 'free-fall' penetration and pop-up requirements of PUPPI meant that the drag should be minimized while maintaining a design which was simple to handle at sea. This necessitates that the weight of the recoverable instrumentation and buoyancy package should be as small as possible. To allow this light construction, the instrument is assembled, handled and launched in the vertical position in order that bending moments, and hence weight, can be kept to a minimum.

Figure 5 shows a sketch of the assembled instrument. It consists of three sections:

1. A top section, containing the buoyancy, the command pinger tube, the data logger tube, a flashing light and the radio beacon which are mounted around a central lifting rod.
2. The centre section comprises the differential pressure transducer, pipe cutter, reed switch for penetration indication and the acoustic/mechanical release assembly all of which are housed in an aluminium cage shrouded by a plastic cover.
3. The bottom section consists of the disposable lead weights, the 3-metre probe with the pressure port at the tip and the penetration indicator (see

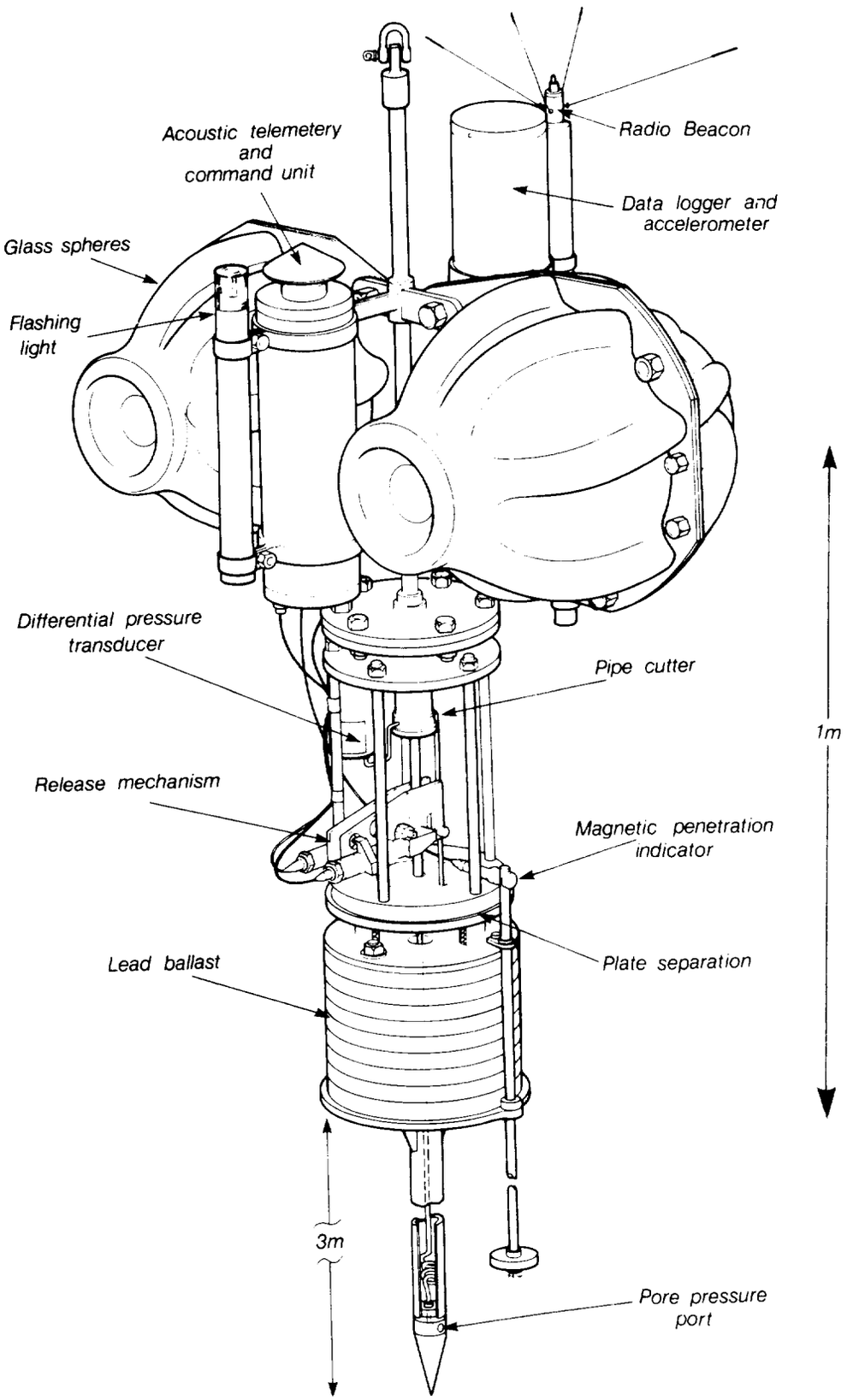

Fig. 5. Pop-Up-Pore-Pressure-Instrument (PUPPI). (The recovery line, plastic shroud and fins are not shown).

Section 10).

The buoyancy of the top and centre sections, which are recovered, is obtained using two 0.43m-diameter glass spheres, each providing 23.3 kg of buoyancy. The excess buoyancy available for ascent to the surface is 13.6 kg. The command pinger is positioned to allow a clear acoustic window to the surface with the data logger pressure housing mounted diametrically opposite to maintain symmetry. A flashing light and radio beacon are used to aid recovery and are located on the outside of the two pressure cases.

The disposable weight stack consists of a variable number of lead weights, each 2.54-cm thick, 30 cm in diameter, and weighing 18.8 kg in air. This adjustable driving force is to compensate for differing sediment strengths. It is desirable that the probe should penetrate up to the lead weight stack for maximum stability in the seafloor. The actual number of weights required will be determined by experience; however, calculations suggest that between four and eight weights should be sufficient for most of the shear strength range encountered with deep sea sediments (see Section 5). The 3-metre probe is a thick-walled steel pipe with a solid tip which contains a porous ceramic pressure port. This pressure port is connected to a 3.2-mm diameter nylon tube which passes up the inside of the probe, through the lead weights and the pipe cutting device and terminates at the differential pressure transducer. When the acoustic mechanical release operates, it separates the top and centre sections from the lead weights. The release plates have been designed to prevent movement in both vertical and horizontal planes during all operations prior to release giving stiffness to the system. Separation is designed to be possible even at angles greater than 45° to the vertical. Simultaneously with this release, the spring-loaded cutter severs the pipe, allowing the top and centre sections to ascend freely to the surface.

To ease relocation of the surfaced instrument, a radio transmitter and flashing light are attached. The radio transmitter, designed by C. Hunter (IOS) is powered from four 'D-size' Lithium Manganese Dioxide cells, and radiates 2W at 150 MHz for up to 20 hours. A range of up to 10 km can be expected. A rotatable directional antenna is used to home in on the transmitter.

The flashing light is manufactured by Oceania Inc. and is activated by a pressure switch, as is the radio transmitter. A buoyant recovery line is folded on top of one of the glass sphere housings and is held in place during the descent phase by corrodable magnesium links.

5. SEDIMENT PENETRATION

In order to determine the mass of ballast weight that would be required to ensure full penetration of the 3-m probe into the sediment, a mathematical model describing the penetration event was constructed. The event can be divided into three stages: (1) cone entry, (2) the entry of the shaft of the probe, and (3) the entry of the weight plate and ballast weights. Ideally, the instrument should be ballasted so that the weight plate enters the sediment and retards the instrument so that the release plate is not buried in the mud. If PUPPI over-penetrated then the buoyancy may not be able to pull the instrument out of the mud on release due to suction forces. Under-penetration could cause the instrument to tilt severely or even fall over.

The mathematical model giving the sediment resistance to penetration used very simple empirical soil mechanics principles. Each horizontal area has an end-bearing pressure given by $N_{cd}.C_u$ where N_{cd} is known as the dynamic end-bearing capacity factor and $C_u = a + bz$ is the undrained sediment shear strength at a depth, z. All vertical surfaces have a frictional shear stress given by $\alpha_d.C_u$ where α_d is the dynamic shaft adhesion factor. For this problem, both N_{cd} and α_d are assumed to be constant. Neglecting the cone friction, as its area is small compared with the shaft, the sediment resistance for the three-stage entry described above can be written,

$$F_1 = A\left(\frac{z}{H}\right)^2 . N_{cd} . C_u\,(z) \quad .. \quad .. \quad .. \quad z < H$$

$$F_2 = A(N_{cd} . C_u\,(z) + \rho_s g\bar{z}) + \pi D\bar{z}\,\alpha_d . C_u(\tfrac{\bar{z}}{2}) \quad .. \quad .. \; H < z < (L + H) \qquad (14)$$

$$F_3 = A(N_{cd} . C_u\,(z) + \rho_s g\bar{z}) + \pi DL\,\alpha_d . C_u\,(\bar{z} - \tfrac{L}{2})$$
$$+ A_1\,(N_{cd} . C_u\,(z') + \rho_s g z') + \pi D_1 . z' . \alpha_d . C_u . (\tfrac{z'}{2}) \quad .. \quad z > (L + H)$$

where $A = \pi D^2/4$ and $A_1 = \pi(D_1^2 - D^2)/4$. Other variables refer to the instrument dimensions shown in Figure 6. The free-fall impact equation is then

$$m_e \ddot{z}^* = W_{nett} - \tfrac{1}{2}\rho \dot{z}^2 (SC_D)_z - F(z) \qquad (15)$$

where ρ = water density, $(SC_D)_z$ = the sum of products of the instrument component projected areas and drag co-efficients for vertical flow, m_e = the effective mass of the instrument, W_{nett} = the nett weight of the instrument in water and F(z) takes one of the three forms in (14) dependent on the value of z. $\ddot{z}^*$ is the instrument acceleration and $\dot{z}$ its velocity. From known and estimated

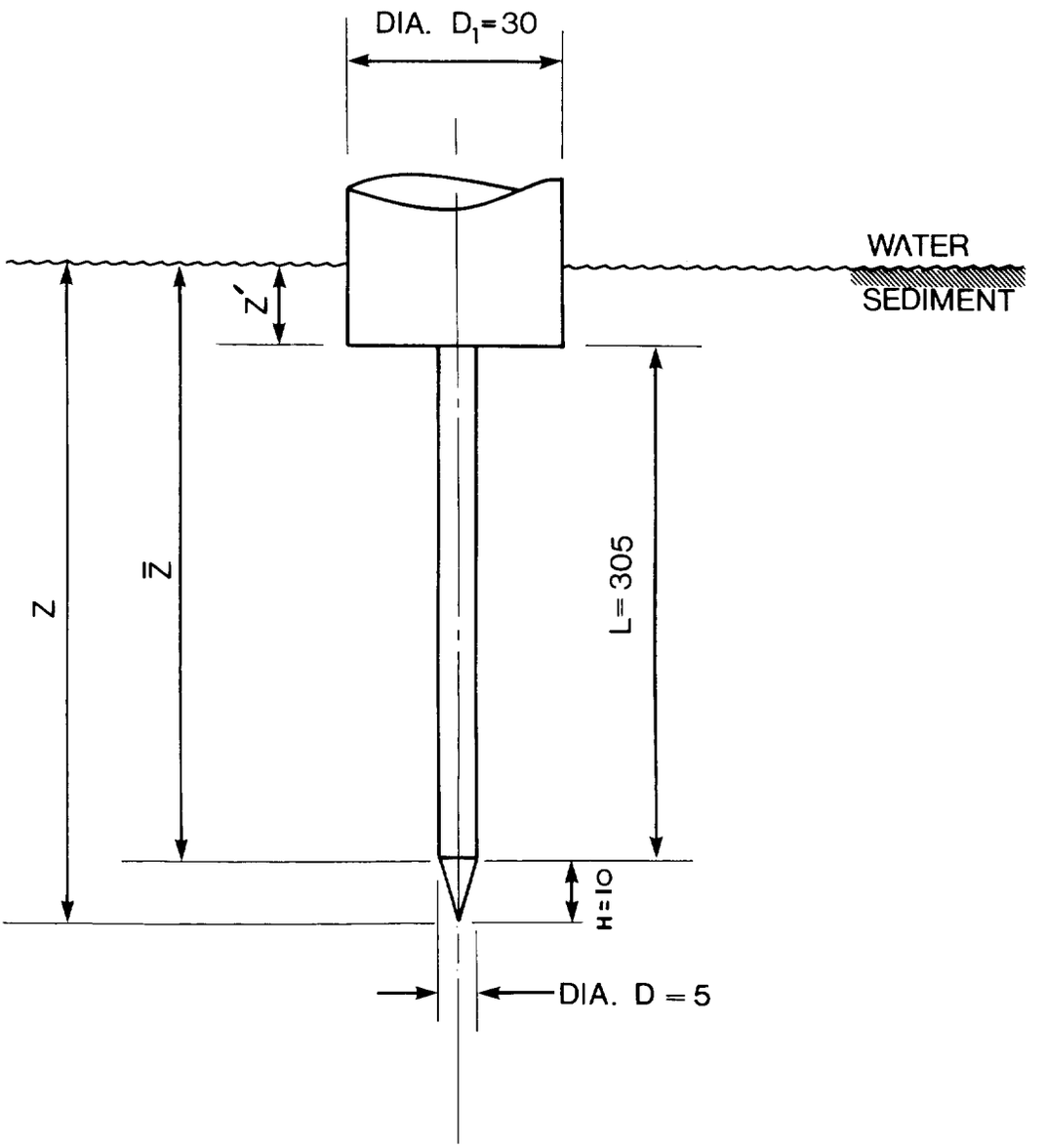

Figure 6: Penetration co-ordinates. Dimensions in centimetres.

component weights in water allowing for the buoyancy of the spheres

$$W_{nett} = 350 + 185n \quad (N)$$

where n = the number of lead ballast weights. The effective mass allowing for the instruments' added mass is given approximately by

$$m_e = 520 + 21n \quad (kg)$$

This latter figure could only be crudely estimated before the instrument trials. The fitting of an accelerometer in the shallow water trials allowed m_e to be estimated more precisely, and this is the value given above. The vertical drag sum $(SC_D)_z$ was approximated from known drag co-efficients for similar geometries or those quoted by manufacturers giving $(SC_D)_z \simeq 0.58\ m^2$. This value was confirmed by the trials to within 10%. The soil co-efficients N_{cd} and α_d were taken from the experimental results of Litkouhi (1979) and Dayal and Allen (1975) for an average penetration velocity of 1 m/s. These results gave $N_{cd} \simeq 14$ and $\alpha_d \simeq 1.2$.

Equation 15 was integrated numerically to examine the dynamics of penetration into sediments with differing shear strength profiles, $C_u(z)$, and for a range of values of n. Figure 7 shows the velocity plotted against penetration of the tip of the probe for three penetrations into a medium strength sediment with different loadings. Figure 8 indicates how the shear strength profile can alter the penetration of an instrument loaded with six weights.

In the stronger sediment, it appears that 8-9 weights would be required to guarantee penetation to the hilt, while in the weak sediment four weights would probably be sufficient. Clearly, a good knowledge of the sediment strength will be required in order to ballast the instrument correctly prior to deployment.

6. HYDRODYNAMIC STABILITY

Clearly, the problem of ensuring that the instrument descends and penetrates vertically can only be examined by modelling the hydro-dynamic pitch stability of the instrument in free-fall. A mass distribution for the free-falling instrument, including its added mass, was assumed and its theoretical pitch centre determined. Then the moment of inertia in pitch, I, was approximated together with the instrument's static righting moment about the pitch centre, M_0; this is due primarily to the buoyancy of the spheres and the weight of the ballast and probe. If the instrument takes on a pitch angle, $\emptyset$, then a lift force, L_p, will be generated by the probe which will act against the righting moment, M_0. Using an approximation for L_p at small pitch angles similar to that given by Hoerner (1958) the equation of motion in pitch for small $\emptyset$, as

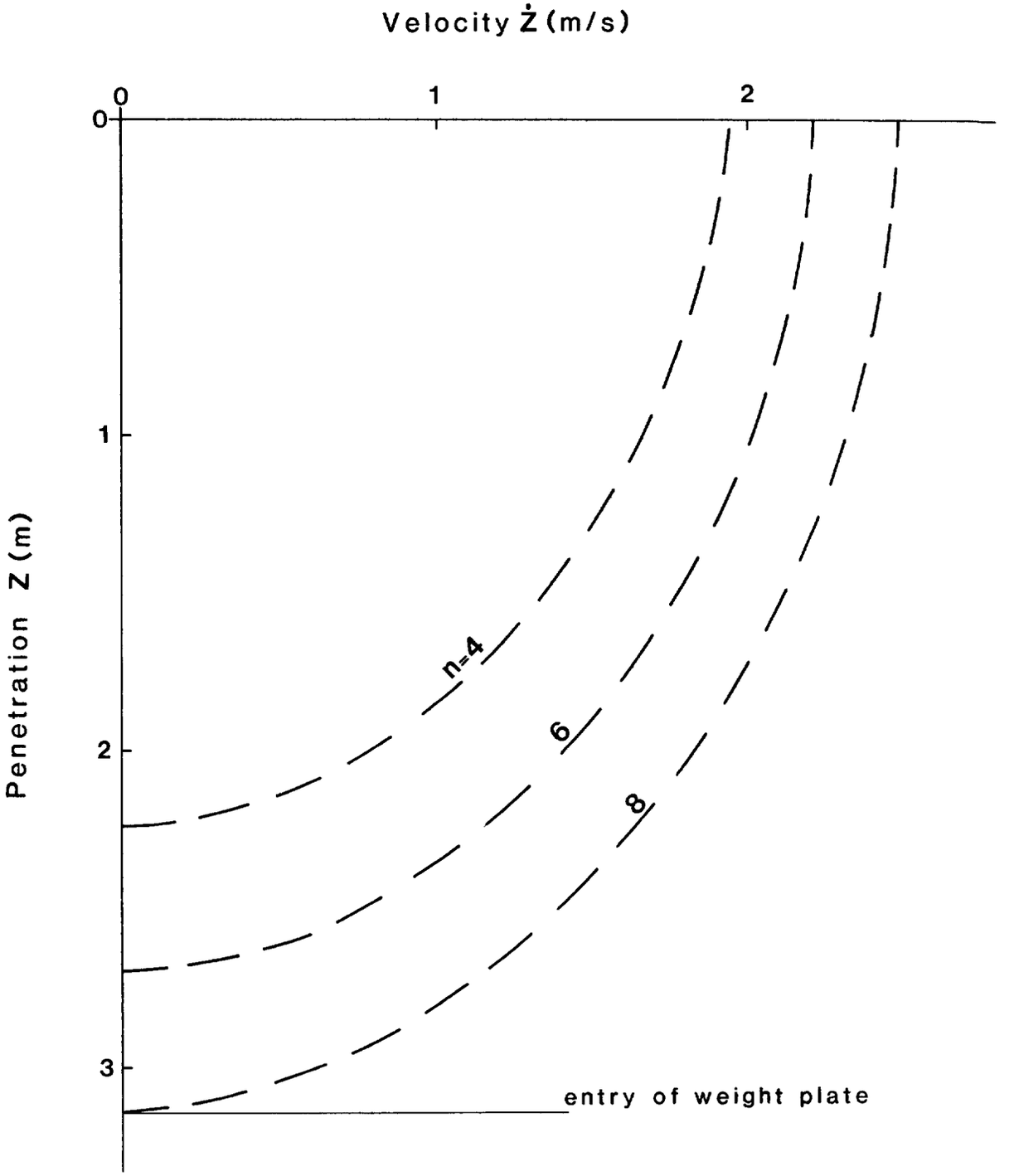

Figure 7: Velocity-penetration curves for a range of ballast loadings for penetration into a sediment with a shear strength profile: $C_u = 3 + 1.2\ Z$ kPa.

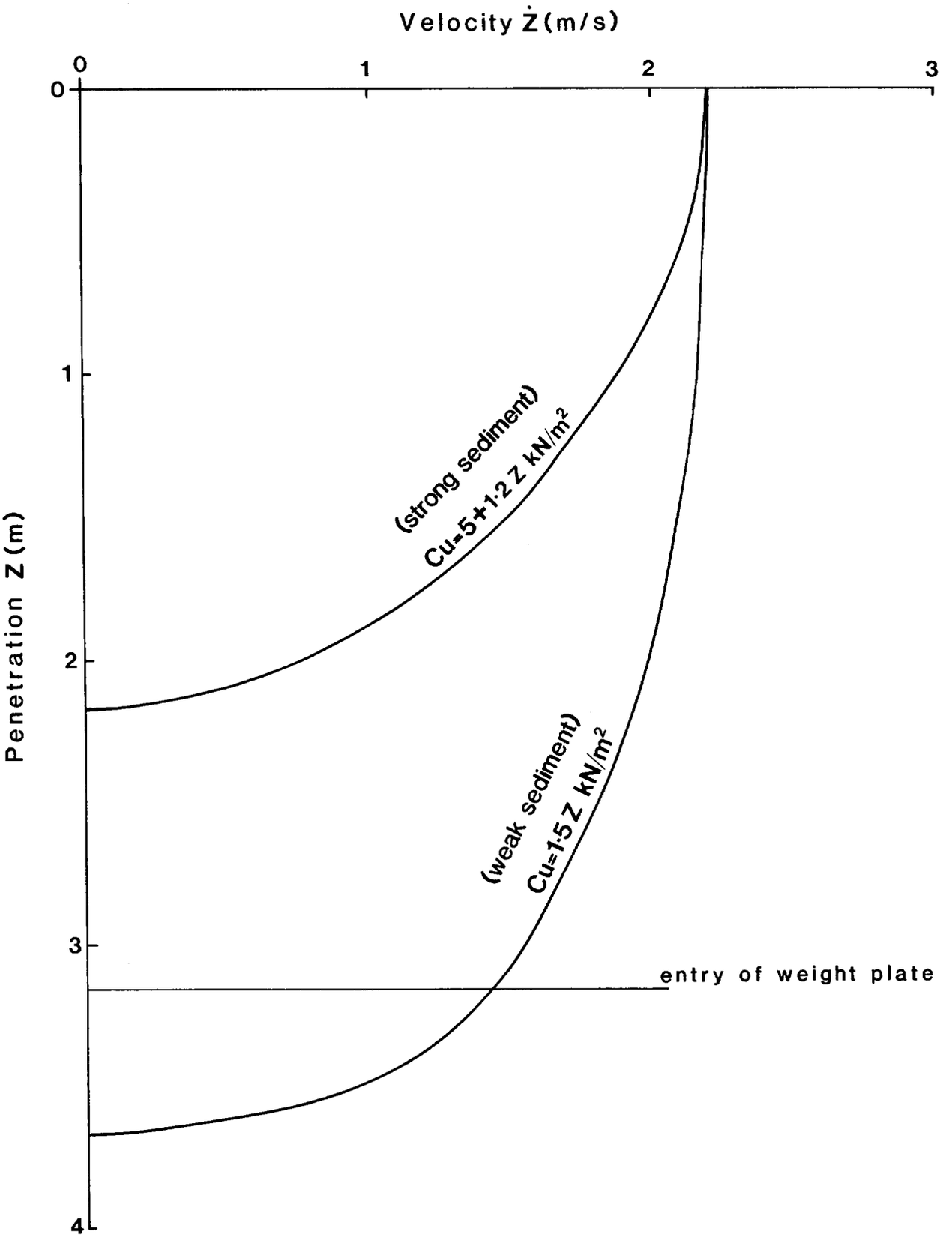

Figure 8: Velocity-penetration curves for strong and weak sediment types. Instrument loaded with six ballast weights.

given below, can be integrated numerically (see Figure 9).

$$I\ddot{\emptyset} = -M_o + x_p L_p \qquad (16)$$

Using this technique, the motion of the free-falling instrument, assuming it had some initial pitch angle, was calculated and the instrument stability deduced. Figure 10a shows the instrument response subsequent to an initial perturbation angle of 0.2 rad (≈11.5°) and for three loading configurations. The response clearly indicates that the instrument as shown in Figure 5 is stable, in that it returns to zero pitch angle, but is under-damped. This means that, due to its oscillatory response, it takes a long time to settle to steady vertical flight. The time of flight at the trials site was 8-9 seconds, see Table 1. So any perturbation received at the surface, i.e. during release, would not have damped out by the time the instrument hit the mud. If this is correct then, had the trials site been three times deeper, better results may have been obtained.

The damping may be increased by the addition of cruciform tail fins at some point above the pitch axis. If the instrument pitches then the tail fins provide a lift force in such a sense as to reduce the pitch angle, whatever plane the angle may be in. The lift force was approximated using flat-plate aerofoil theory making some allowance for the small aspect ratio of the fins. Two configurations were investigated and the results are shown in Figure 10b. The figure shows some quite large fins mounted on a 2.1m tail arm, S_f is the fin area, shown shaded in the sketch. This configuration has a highly-damped response shown for a loading of eight ballast weights by the solid line. The response takes more than ten seconds to reach equilibrium. This can be speeded up by reducing the fin size and reducing the length of the tail arm.

For a number of reasons it would be convenient to mount the fins at the level of the spheres. There are convenient fixing locations there which means that no additional structure, with its associated weight penalty, need be attached to the ascent part of the instrument. Also, by fixing the fins at the correct height, no destabilizing turning moment will be imposed on the instrument on its ascent. Configuration 1 on Figure 10b shows this arrangement. The fin size, S_f, was reduced to give critical damping which reduces the time to get back to equilibrium to about five seconds. This solution is shown dashed on part of Figure 10b.

By lead filling the hollow probe, the weight distribution of the instrument could be significantly altered to increase the static righting moment, M_o. Approximately 42 kg of lead could be relocated in this way which is equivalent to

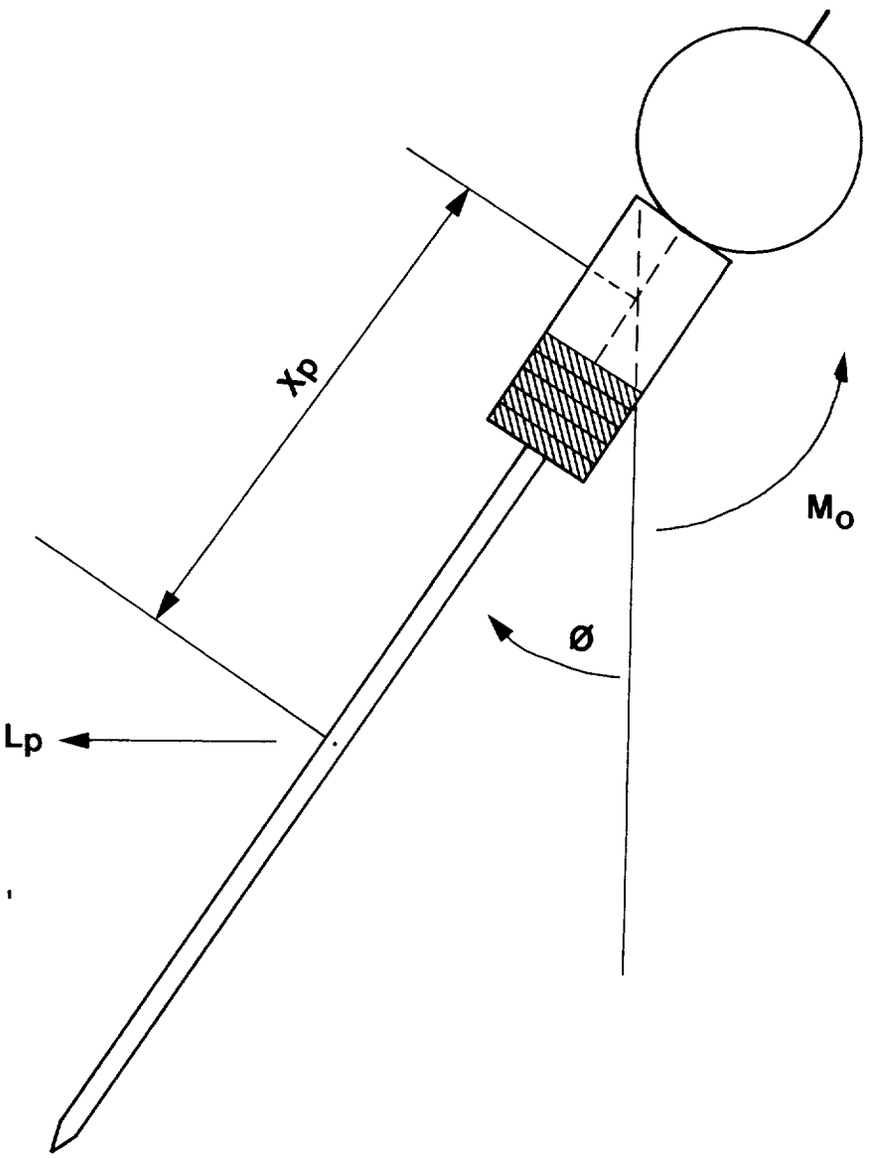

Figure 9: Hydrodynamic pitch stability of PUPPI.

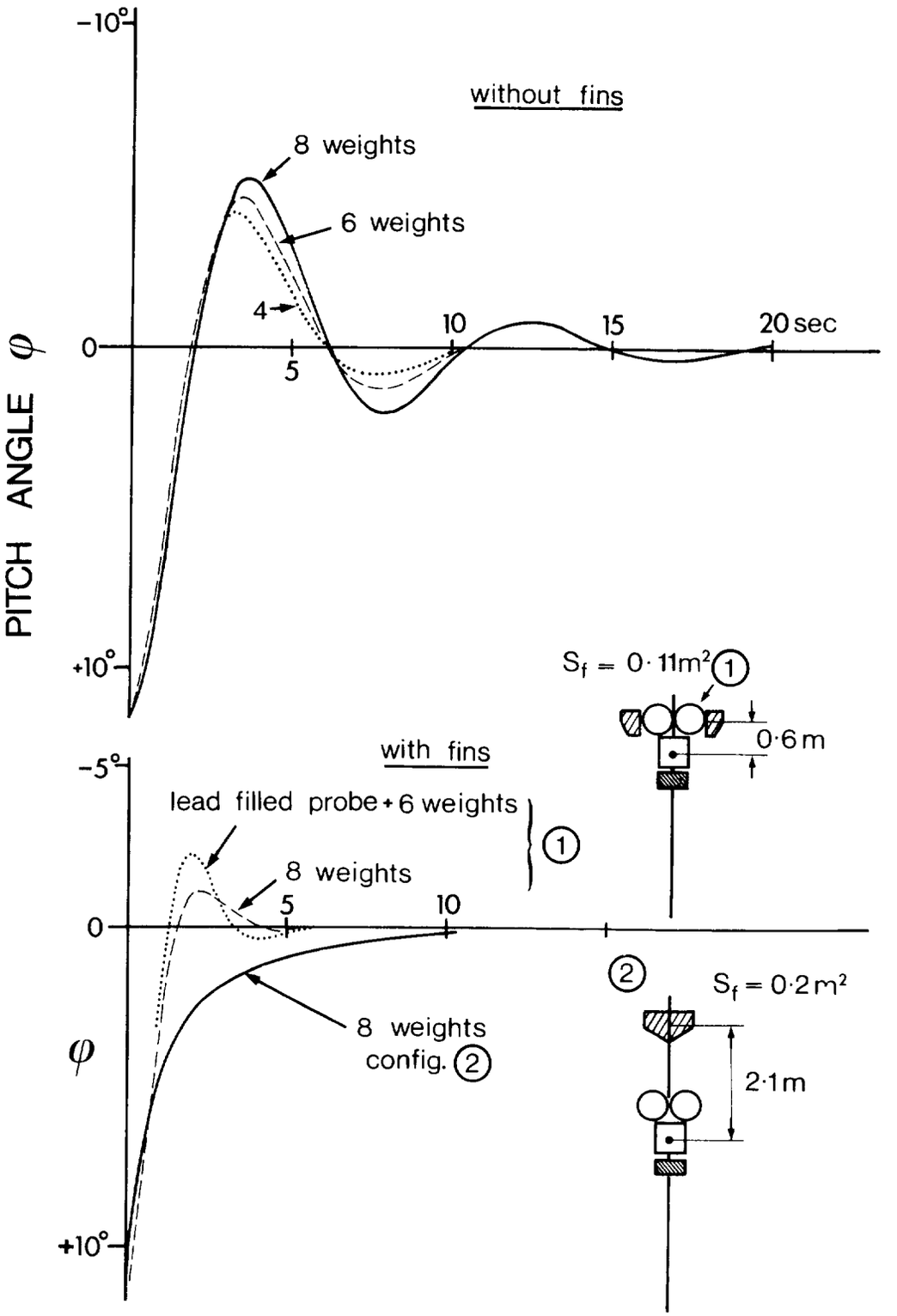

Figure 10: Instruments response characteristics to an initial perturbation of 11.5° (0.2 rad); (a) without fins, (b) with fins. The response curves are shown for different numbers of ballast weights and with different fin configurations.

two of the lead ballast weights. This would increase M_0 by 27%, it also increases the moment of inertia and lowers the pitch axis slightly. The changed response curve for this arrangement with the fins as for configuration 1 is also shown in Figure 10b. The response is faster but the overshoot is higher. Further calculation has shown that for this arrangement critical damping can be regained by increasing the fin area, S_f, to 0.2 m^2. The sizes of these fins for critical damping and arrangements for fitting them to the instrument are shown in Figure 11. It should be noted that the detailed hydrodynamic stability analysis was only initiated after problems of tilt had been encountered during the shallow water trials. Consequently the fins were only fitted for the deep water trials.

7. DIFFERENTIAL PRESSURE TRANSDUCER

The differential pressure transducer (Appleby and Ireland, Multitron 741DD) was chosen for robustness and compatibility with the harsh operating environment. Figure 12 is a simplified drawing of the transducer with the modifications necessary for use at ambient pressures of 9000 p.s.i.

Differential pressure is applied across a diaphragm which flexes, moving a ferro-magnetic core within a 'Linear Variable Differential Transformer' (L.V.D.T.) assembly. The primary coil windings of the transformer are excited by a 1 kHz sinusoidal current and the output from the secondary coil windings is directly proportional to the displacement of the core.

The L.V.D.T., unlike a strain gauge transducer, has no mechanical linkage between the moving part (the core) and the electrical system. There is little friction to impede the motion of the diaphragm and so the hysteresis of the transducer is low. As the transformer is completely potted it is able to withstand high ambient pressures and is inherently robust.

The cavity around the L.V.D.T. is filled with oil so that ambient pressure is maintained, allowing operation at water depths of at least 6000m. A rubber boot compensates for changes of volume due either to the thermal expansivity or bulk modulus of the oil, or that of any entrapped air. 'Mentor' oil was chosen for its low thermal expansivity, and its relative ease of handling.

A 'transducer' of range ±200 kPa was used to accommodate the possibly large differential pressure produced when the probe penetrates the sediment.

Because of the effect of ambient pressure and temperature upon the zero offset, it is not possible to calculate accurately (from laboratory measurements) the 'true zero' for recovered data. A zero reference can be obtained, however,

a, FIN SIZE FOR PRESENT PUPPI WEIGHT DISTRIBUTION

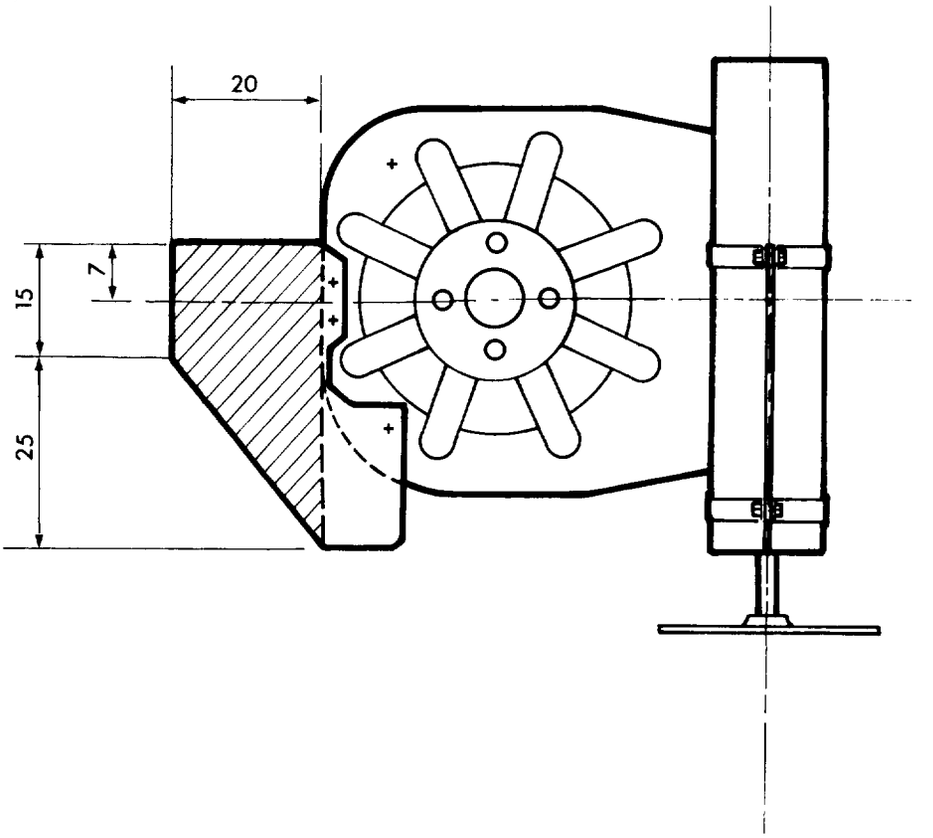

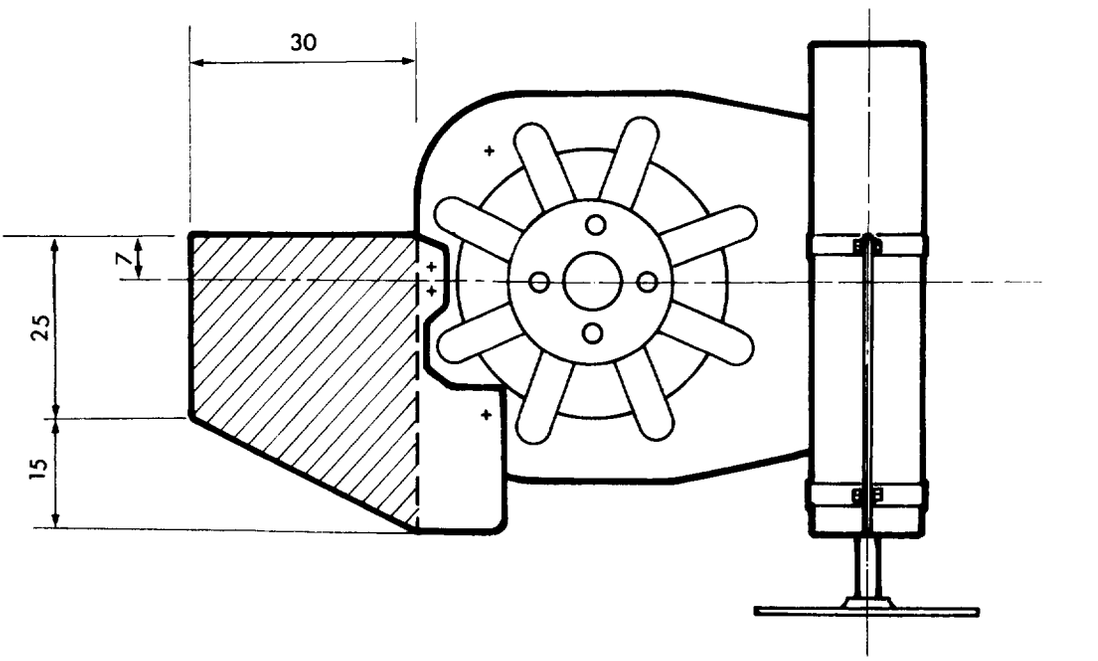

b, FIN SIZE CRITICAL DAMPING OF THE LEAD-FILLED PROBE VERSION. DIMENSIONS IN CM'S

Figure 11: Fin configurations.

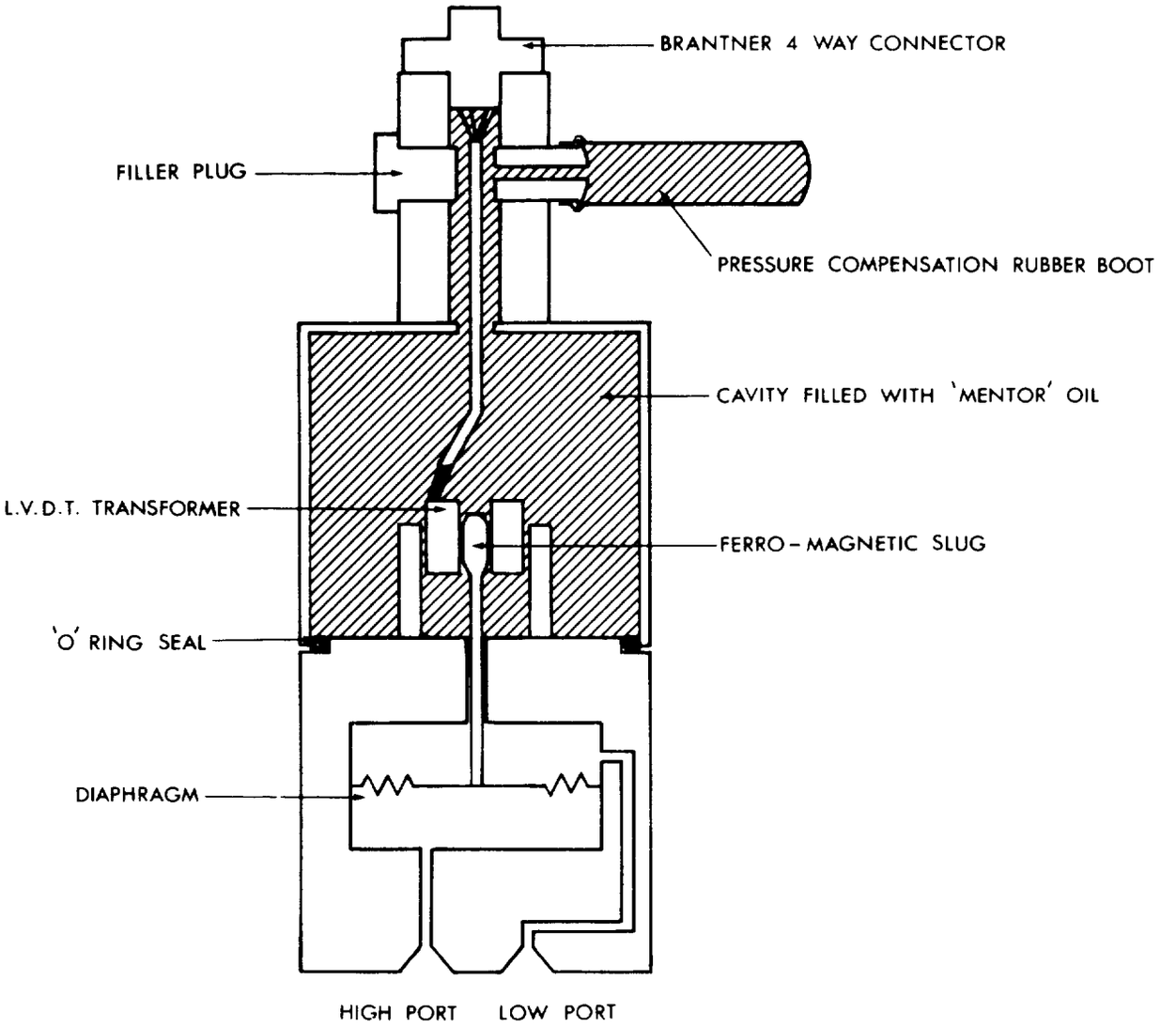

FIG.12. DIFFERENTIAL PRESSURE TRANSDUCER MULTITRON TYPE AI 741 MODIFIED FOR USE AT AMBIENT PRESSURES OF 9000 P. S. I.

just prior to the release of the instrument from the sea bed when the pipe joining the high port to the probe tip is cut. With this reference, the resolution will be limited by the hysteresis of the transducer and the quantisation error of the analogue to digital conversion. Laboratory tests of the transducer have shown that the hysteresis error is less than the quantisation error of a 13-bit digitisation.

8. DATA LOGGER

The requirement of the data logger is to record the differential pore water pressure induced in the sediment as the probe is inserted, to measure the decay as this pressure pulse dissipates, and to quantify any residual differential pressure associated with pore water movement.

The data recorder is required to log several thousand pressure readings over a period of several days (perhaps weeks), hence it was decided to use a solid-state EPROM logger to record the data.

The advantages of an EPROM logger over the alternative tape cassette logger are:

1. Robustness. There are no moving parts.
2. Ease of replay. Data can be transferred quickly with a minimum of additional hardware.
3. Savings in weight and volume.
4. Cost. The replay systems for cassette loggers are particularly expensive.

An EPROM logger has the disadvantage of having a much smaller data storage capacity; e.g. the PUPPI logger has a capacity of 256K-bit compared to 14M-bit for the Sea Data logger. However, for PUPPI, the capacity afforded by the EPROM logger is more than sufficient.

The data recording system is shown in Figure 13. The high pressure port of the differential pressure transducer is connected by the nylon pipe to the porous pressure port at the tip of the 3-metre long probe. The other transducer port is left open to ambient hydrostatic pressure. Consequently, the pressure sensed by the transducer is due entirely to the differential pore water pressure at the tip of the probe relative to ambient hydrostatic pressure. An underwater cable connects the transducer to the data logging package.

8.1 Transducer Interface

The transducer interface electronics provides a.c. excitation to the

FIGURE 13. P.U.P.P.I. DATA RECORDING SYSTEM

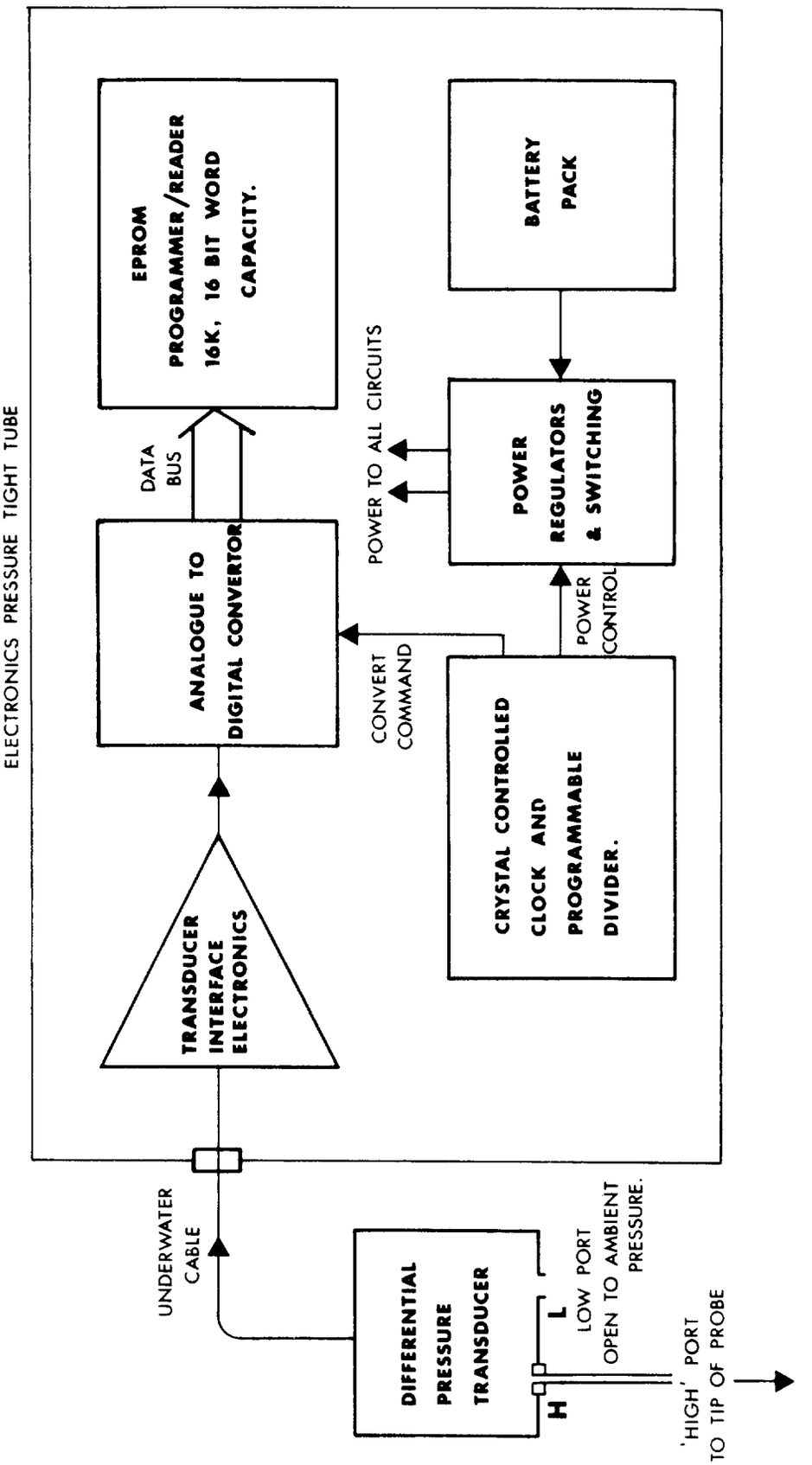

transducer and detects the returned signal, generating an output voltage proportional to differential pressure.

The relatively high power consumption of 25 mA at ±5V necessitated that the interface electronics was powered on for only one second before the pressure reading was digitised and stored. A programmable clock circuit determines when a pore pressure measurement is to be made and also controls a power supply switching circuit providing power to the appropriate circuits only when needed. The time constants in the signal filters were chosen so that the output voltage settles to within 0.01% of its final value after one second.

8.2 Analogue-to-Digital Convertor

An ICL7901 integrating analogue-to-digital convertor (ADC) giving 13-bit resolution is used. The ADC works ratiometrically with the L.V.D.T. interface, as the reference for the stabilisation of the L.V.D.T. excitation, and the ADC reference are both the +5 volts supply. As with the L.V.D.T. interface, power is applied to the ADC for only one second for each measurement. Tri-state buffers are used to present data to the EPROM logger for the 50ms "burning-in" period.

8.3 Clock and Programmable Divider

The clock circuit sets the sampling rate which may be pre-set to vary throughout the instrument's deployment.

A one-second pulse, derived from a crystal oscillator, is divided down according to a matrix, preprogrammed with diode shorting pins. The deployment is split into ten "time frames". For each frame, the sampling interval can be set from two seconds to 2049 seconds. The number of measurements within that frame can vary from 10 to 1280. After the last sample of a time frame, the next frame is read.

For example, the diode pins might be arranged to give:

FRAME	SAMPLE INTERVAL (s)	NUMBER OF SAMPLES
1	2	1000
2	30	1500
3	60	100
4	100	700

This flexible sampling-rate programming, allows the available data storage

capacity to be used most efficiently. After the ADC has made a conversion, a pulse is generated, commanding the EPROM logger to record the data.

8.4 EPROM Logger

Addresses in two EPROMs are programmed in parallel for each word which is 16-bits long. Four NMOS2764, 64-K bit EPROMs can be programmed during each different deployment giving a storage capacity of 16K, 16-bit words. As the stand-by power consumption of the EPROMs is high (100 mA at 5V), power is applied to the EPROMs only for the 50 ms required for programming an address.

Zero insertion force sockets allow the EPROMs to be easily interchanged.

8.5 Power Supply

The power supply provides a switched ±5 volt supply to the ADC and Transducer Interface, and a switched 5.2 volt and 21.2 volt supply for the EPROM Logger. These supplies are switched on for 1.5 seconds on command from the clock. A constant 5-volt supply is provided for the clock circuits and CMOS logic in the ADC and EPROM logger. Current consumption by these circuits is very low (<0.5 mA), and so, to obtain maximum possible battery life, a voltage regulator with negligible quiescent current is used. The -5 volt supply is obtained by the use of a voltage invertor. This simplifies battery requirements. Three MN1604 9-volt batteries generate the 27-volt supply needed for programming, and a 9-volt battery pack, consisting of three L032S 1.1 A hr. 3-volt cells, is used for all the other supplies. This battery pack will power the logger for 1000 hours.

8.6 Replay System

The most convenient way to display the data for a quick look is to play it out as an analogue record on a pen recorder. The replay system (Figure 14) plugs into the EPROM logger board via a 40-way connector and converts the binary words back into analogue voltages. The EPROM address for each sample is displayed (in HEX).

Clock pulses are generated within the replay system at a switch selectable rate of 3 Hz to 1000 Hz. The pulses are divided down by the programmable divider in the clock circuit of the data logger. With the diode pins set as during the deployment, the data output is a time-compressed replay of the recorded pressure readings and the time scale is linear. A time code is generated from the clock pulses which is played out with the data.

FIGURE 14. P.U.P.P.I. REPLAY SYSTEM

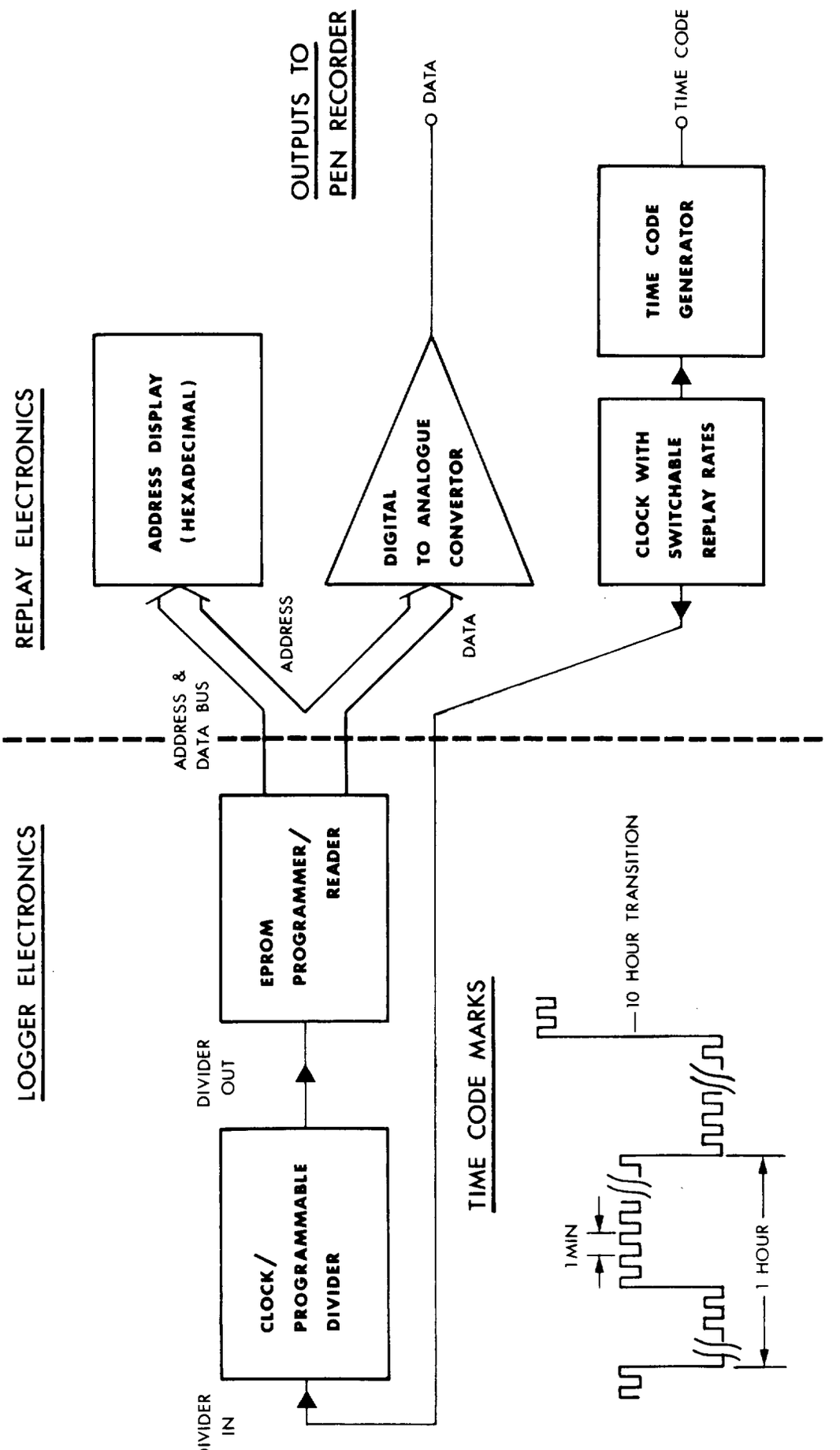

The EPROM data is also loaded into a PET micro-computer memory via the parallel user port, and then onto a mini floppy disc for data handling and storage.

The EPROMs themselves are U.V. erasable and so could be re-used. However, the relative cheapness of the EPROMs (#30 per deployment) does not normally warrant their re-use.

8.7 Back-up Release Timer

This is incorporated as a back-up should the acoustic release system fail. The timer may be set to fire after a delay of one to 256 hours. A cable connects the output of the timer to the acoustics tube where the pyro-firing circuits are diode mixed.

9. COMMAND PINGER

The acoustic command pinger and release system enables the instrument to be monitored through the water column and while in the sediment. It also provides the current required to operate the pyro-releases on command from the ship enabling the instrument to ascend to the surface. All aspects of this system are described in detail by Phillips (1981).

9.1 Acoustic Telemetry of Tilt and Penetration

Each deployment of PUPPI will involve a degree of uncertainty as to what it may hit on the seafloor. Consequently, real-time information is required about its tilt angle and penetration. On the basis of this information, it can be quickly decided whether to release immediately and recover the instrument or to leave the instrument to record the pressure data.

Tilt is telemetered acoustically by gating extra pulses through the command pinger. The tilt sensors use mercury and two electrodes in a glass phial to make or break an electrical circuit (Phillips, 1981). Five discrete sensors are used to indicate angles greater than 10, 15, 20, 30 and 60 degrees from the vertical.

Indication of penetration is at present limited to knowing whether the probe has penetrated more than 2.5 metres. At penetrations greater than 2.5m a plate attached to the bottom of a vertical bar, slides up the probe. A magnet, mounted at the top of the rod, moves away from an encapsulated reed relay. This provides another gated pulse which is telemetered by the command pinger.

This system, however, does not provide any accurate penetration data which

is required (a) to calculate accurately the differential pore pressure gradient; and (b) to predict accurately the number of ballast weights required for different sediment types. Under-penetration could leave the probe in an unstable position and over-penetration could clog up the release mechanism or cause suction forces that would make release impossible.

10. ACCELEROMETER

To monitor accurately the behaviour of PUPPI, it was instrumented with a vertically-mounted accelerometer. It was intended that the deceleration record prior to, during and after penetration would provide valuable information on the behaviour of the instrument both in the water and the sediments.

The numerical modelling of the penetration event (see section 5) had indicated that a 1g accelerometer would have an adequate range to cover the expected peak decelerations. The accelerometer trace of the penetration event would, on integration, (w.r.t. time) give the velocity profile and, on double integration, the depth of penetration. (Terminal velocity could also be obtained from the initial drop.) The accelerometer can also record the final tilt angle. However, the cosine response to tilt means that, at small angles, it is not very accurate.

One immediate problem realised was one of data storage requirements. A sampling rate of greater than 50 Hz would be required and almost an hour's worth of data would have to be stored, assuming recording was started at the beginning of the descent. This works out at over 100 K bytes of data which cannot be stored in the EPROM logger, or any other practical solid state logger. A cassette logger would have the required capacity but would be a rather expensive and bulky addition to the electronics package.

The solution was to store the data in a RAM which continually overwrites itself so that, at any one time, the last minute of the record is stored in the memory. The penetration of the probe is detected and the logger stops sampling, so that the last minute of data, which should include the deceleration of the probe, is 'frozen' in the memory.

The penetration of the probe is 'sensed' indirectly by a circuit which looks for the period of low vibrational noise experienced after penetration (when the instrument has come to rest) compared to the relatively high levels of vibration during the descent or when on the ship. It was found that, during the Oban deployments, the vibrational noise levels were several orders of magnitude less, with the probe at rest in the mud, than during the descent.

A block diagram of the accelerometer logger is shown in Figure 15. An accelerometer of the variable relutance (Schaevitz A411-001) is vertically mounted. The output is anti-alias filtered at 30 Hz and converted to 8-bit words at a rate of 128 Hz which are stored on a 8K-byte RAM with its own battery back-up (type IR 2364 from Greenwich Instruments). The memory is continuously overwritten so that, at any one time, it contains 64 seconds of data.

A threshold detector resets an interval timer when the vibration exceeds a pre-settable level. If the vibration does not exceed the threshold for a period of 36 seconds, the timer times out, resetting a latching relay, switching off power to the logger. The last 64 seconds of data are now stored in the logger. If the noise detector has functioned correctly, the penetration event should be 36 seconds before the turn-off.

Upon recovery, the logger is switched to the read mode, the data is converted back to an analogue signal and replayed on a pen recorder. Integration of the penetration can then be done graphically.

The accelerometer senses the gravitational field and so is sensitive to inclination. The residual acceleration, Δg, at the end of the record is a measure of the final tilt angle, θ,

$$\text{where} \qquad \Delta g = g - g \cos \theta$$

$$\text{therefore} \qquad \theta = \cos^{-1}(1 - \frac{\Delta g}{g}) \qquad (17)$$

where g is the acceleration due to gravity.

Hence the accelerometer can be used to measure the final inclination of PUPPI. For small inclinations, the quantisation of the signal introduces significant uncertainties, as set out in the table below:

INCLINATION	QUANTISATION ERROR
5°	±3°
7°	±2°
10°	±1.35°
15°	±0.9°

11. SHALLOW WATER TRIALS

To test all the systems associated with PUPPI, except the acoustics, a series of shallow water trials was conducted in the Firth of Lorne, 5 miles north of Oban in August 1983. The site chosen was in approximately 20 metres of

FIGURE 15. ACCELEROMETER PENETRATION INDICATOR

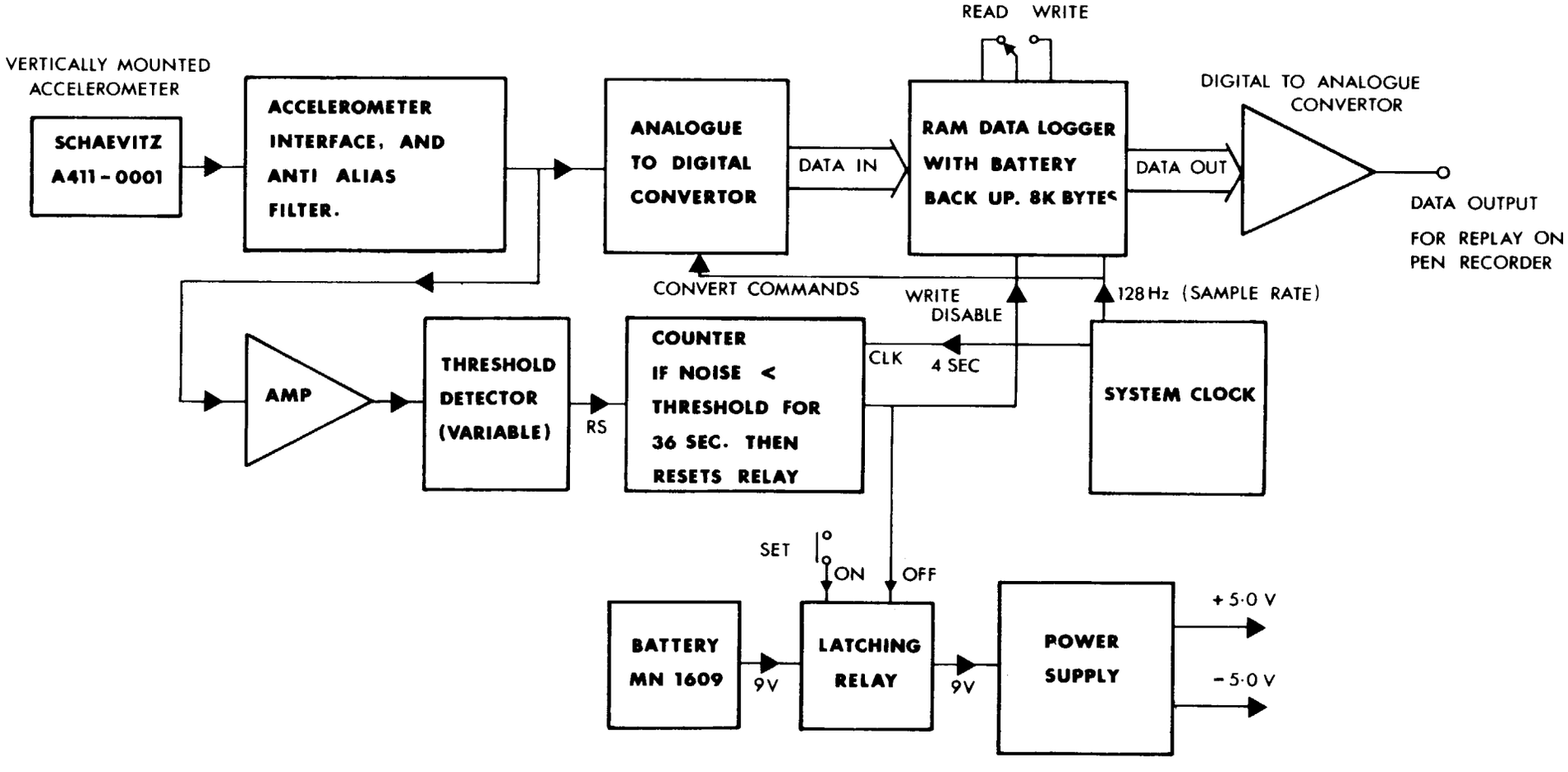

water and the sediment was a soft silty clay (not unlike pelagic clays in consistency) which extended for at least four metres. A gravity core had shown the clay to be very homogeneous throughout the full length. With only 20m of water, it was possible to use divers to (a) observe the free-fall stability; (b) measure the penetration and the tilt angle; (c) release the buoyant package; and (d) attach a warp to the lead weights and probe for recovery. The trials were conducted aboard R.V. Calanus from the Scottish Marine Biological Association at Dunstaffnage. PUPPI was assembled on an extended section over the stern of the vessel and launched using the crane.

11.1 Penetration and Stability

Ten deployments were made with no fins or lead ballast in the lance but using different numbers of lead ballast weights. A summary of the results obtained from the trials is given in Table 1. The site near Oban was selected for the trials because the sediment there had the required characteristics and the depth of water (≈20m) was convenient for diver operations. Integration of the free-fall equation of motion for the vehicle indicated that it would accelerate to terminal velocity in less than 5m. Hence, on dropping the immersed instrument it would have approximately 10m free-fall at terminal velocity before the probe entered the mud. Since the sediment at the site was judged to be of medium-to-weak shear strength, the instrument was loaded first with six ballast weights. Thereafter, various loadings n = 4 to 8 were experimented with. Table 1 indicates that all loadings n = 5 to 8 penetrated to the hilt and just beyond and in no case did the instrument over-penetrate. The maximum penetration for n = 8 gave a penetration of the weight plate of 99 mm, i.e. almost half-burying the lead weights. Only in the cases with n = 4 did the instrument under-penetrate, the degree of penetration varying considerably in the two drops. The best results at the trials site were consistently obtained for n = 6. This loading gave penetration to the hilt with the smallest measured tilt angles.

It is clear that achieving the desired depth of penetration into this type of sediment will not be a problem provided the number of weights is greater than four. The weight plate provides an adequate braking force preventing over-penetration for the range of instrument loadings investigated. The problem remaining was that of achieving straight penetration of the sediment so that disturbance of the mud could be kept to a minimum. This was realised in only two of the ten experimental drops. It was thought that, since the instrument

Table 1 Data from the PUPPI shallow water trials

Drop #	# Weights	Probe	Accln trace	Measured by divers			Calculated from acceleration traces						
				Tilt Angle (deg)	Penetr'tn (in) from plate	Descent time (sec)	Tilt Angle (deg)	Penetration (in) from plate Z'		Terminal velocity (m/s) U_T			Velocity @ plate entry (m/s)
				ϕ	Z'		ϕ	Double int'gn	Int'gn of plate penetr'tn	Int'gn of drop curve	Int'gn of penetr'tn curve	Theoretical	
1	6	S	✓	5	$1\frac{1}{2} \rightarrow 2\frac{1}{2}$	-	0	8	2	-	1.86	2.2	0.79
2	6	S		0	$2\frac{1}{2}$	-	-	-	-	-	-	-	-
3	5	S		10	$2\frac{1}{2}$	9	-	-	-	-	-	-	-
4	4	L		15	$-1\frac{1}{2}$	-	-	-	-	-	-	-	-
5	7	L		14	2	-	-	-	-	-	-	-	-
6	6	L	✓	0	$2\frac{1}{2}$	8.5	0	45	3	-	2.19	2.2	1.03
7	4	S	✓	25	-12	-	17→18	18	-	2	1.33	2.0	-
8	7	S		6	$3\frac{1}{2}$	-	-	-	-	-	-	-	-
9	8	S	✓	18	$3\frac{3}{4}$	-	16	-	$3\frac{3}{4}$	2 2.4 ext	1.13	2.5	1.13
10	7	S	✓	19	$1\frac{1}{4}$	-	17	16	$2\frac{1}{2}$	-	1.75	2.3	0.73

S = short conical probe

L = long slender probe

ext = extrapolated

came to rest at an angle greater than 5° in most cases, it must have adopted some small initial angle before entering the sediment. The increased drag of the nose of the probe entering at an angle would induce a turning moment tending to increase the tilt angle from the vertical. Hence, any quite small pitch angle that the instrument adopted in the water would be magnified on penetration. The time of flight at the trials site was 8-9 s, see Table 1. Hence, according to the results of section 6 shown in Figure 10, any perturbation received from the surface would not have damped out by the time of penetration. If the site had been deeper or if fins had been fitted, better results might have been obtained. Overall, the conclusions reached were that some instability did exist during free-fall which could cause tilt angles in the sediment to approach up to 30°. However, the amounts of ballast required was approximately correct and for this sediment six weights was the optimum number both in terms of penetration and tilt.

11.2 Accelerometer records

Three sample accelerometer traces are shown in Figure 16 covering the range of ballast weights investigated during the shallow water trials (see Section 11.1). The differences in travel time are caused not only by differences in terminal velocity but also by changes in water depth resulting from a tidal range of approximately 2m. At the instant of drop, the amplifier saturated in most cases (as indicated by the hatched line) therefore, the peak acceleration was unrecorded. However, the tails of these acceleration curves can be fitted using the theoretical relationship for the instrument's acceleration from rest,

$$\text{accel} = \frac{W_{nett}}{m_e} \operatorname{sech}^2 \left(\frac{W_{nett}}{m_e} k\right) t \qquad (18)$$

where $k = \rho(SC_D)_z$, t = time from drop and the remaining variables are as described in Section 5. Since W_{nett} is known values of k and m_e can be chosen to give the best fit to the measured acceleration curves. This was done for drops number 7 and number 9 and confirmed the value of $(SC_D)_z$ given in Section 5. The value of m_e estimated prior to the trails was found to be 30% too low by this technique and was revised to give that also shown in Section 5. The accelerometer traces in Figure 16 clearly show the penetration of the weight plate where this occurred. Tilt angles calculated from equation 17 are shown in Table 1.

Integrating both the area under the drop acceleration curve and the area under the penetration deceleration curve yields separate estimates for the

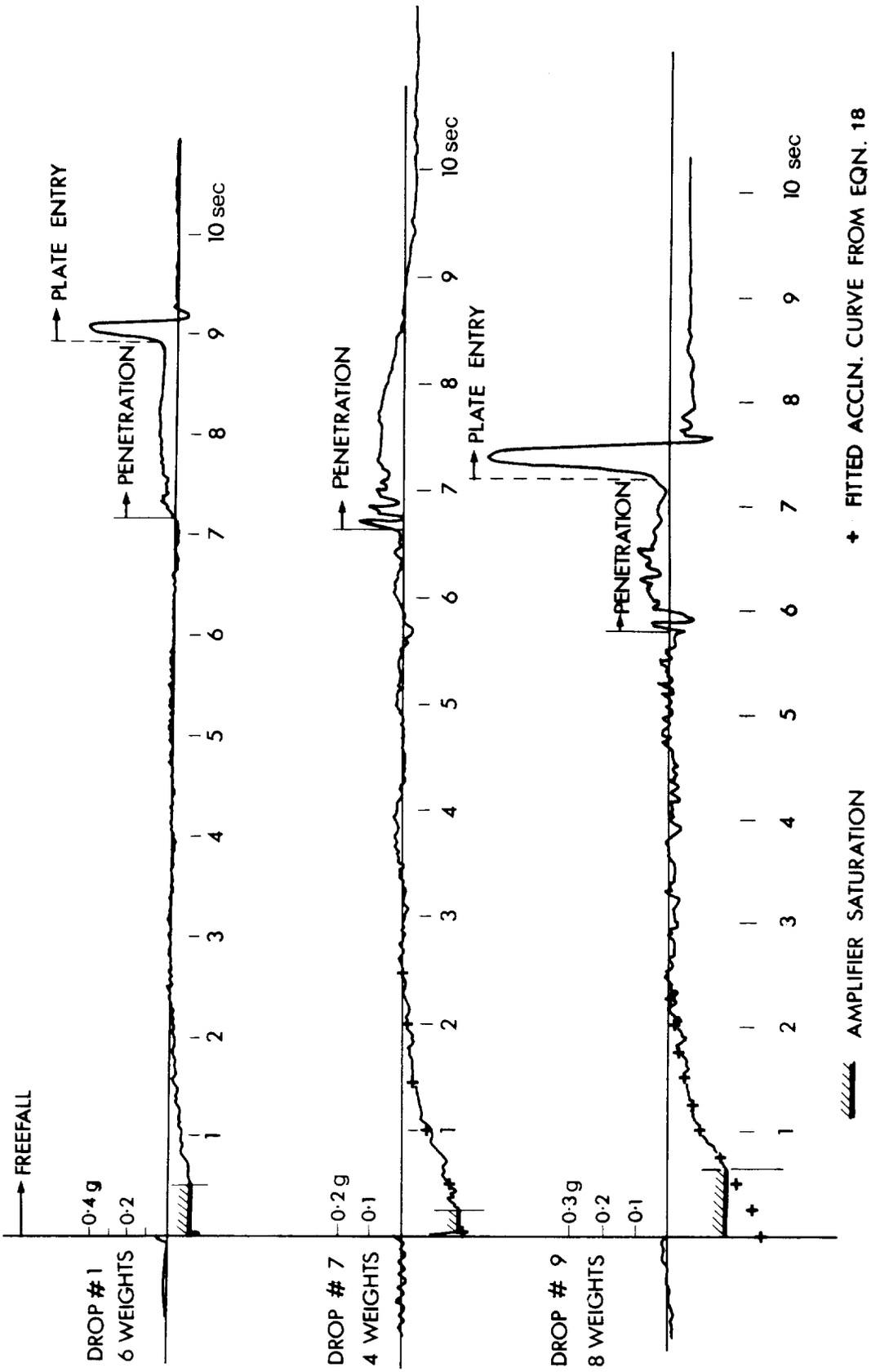

Fig.16 Accelerometer traces from trials with 3 loading configurations

instrument terminal velocity which can be compared with the theoretical value given by

$$U_T = \frac{2W_{nett}}{\rho(SC_D)_z} \qquad (19)$$

These comparisons are also made in Table 1 and it is noted that the results obtained from integrating the drop curve agree better with the theoretical value, when extrapolated to the missing maximum, than the integrations of the penetration curves. Also, double integration of the whole penetration curve gave penetrations far in excess of those measured (see Table 1). For the cases where the weight plate penetrated, it is possible to improve the accuracy of the penetration calculation by integrating the well-defined area under the plate deceleration curve to give the plate entry velocity. Using this, a mean deceleration can be deduced and then Newton's laws give a reasonable approximation to the plate penetration. The penetrations resulting from this calculation are shown in Table 1 under the column marked "Approx. double intgn of plate penetr'tn".

The fact that the instrument penetrated the sediment at an angle in many cases must influence these calculations. The tilted accelerometer would record reduced decelerations which explains why the integrated terminal velocities given by the penetration curves were lower than theoretical in the cases where appreciable tilt was measured. If the instruments were made to penetrate vertically, better penetration results may be obtained. The greatest source of error in calculating the penetration comes in detecting the instant of probe entry. A small error in this when the instrument is travelling at 2-3 m/s results in large errors in penetration depth. The deceleration of a slender cone penetrating the weak surface sediment is very small. Hence, the accelerometer is probably not the best instrument to measure penetration, especially in weak sediments. A direct measuring instrument would be more reliable. Also, the accelerometer, as fitted, is poor at recording tilt angles less than 10°. A pair of more sensitive accelerometers mounted horizontally at right angles would accomplish this function with greater accuracy. However, the accelerometer did yield some valuable information about the trials. Noteably, it gave a check on the estimated instrument drag and it enabled the added mass term to be corrected. It also clearly showed whether the weight plate entered the sediment or not and indicated when the instrument took on large tilt angles. Improved instrumentation to measure tilt and penetration may be fitted as it becomes available but, until such a time arrives, the present accelerometer serves a useful function.

For a deployment in deep water, the terminal velocity of PUPPI will be known with high accuracy (by timing the descent) and this can be used in the penetration calculations thus improving the accuracy considerably. It will effectively mean that only the shape of the acceleration record is important, as the scale will be set by knowing the initial velocity (V_T) and the final velocity (zero).

11.3 Pressure measurements

Differential pressure was successfully recorded for all ten deployments. The data logger functioned faultlessly throughout the trials. Figure 17 is the differential pressure record obtained for drop number three and illustrates the type of data obtained. The large negative pressure at the beginning of the record is caused by trapped air in the system that was not expelled during bleeding. During descent, the ambient pressure increases rapidly and any gas undergoes a volume change proportional to that pressure. This involves movement of water through the porous stone and along the pipe connecting it to the transducer. The pressure decreases during descent because water takes longer to move through the porous stone and pipe than it does through the open port. In deep water the pressure would be back to zero long before the instrument reached the bottom, even if the system was not bled at all.

As a result of the negative pressure that had been 'locked in' during descent no immediate positive pressure caused by penetration can be observed Instead, the pressure slowly decays towards zero (in this case, it took more than six hours). The oscillation in pore pressure at the end of the record is attributed to the tidal effect on the system containing some air (gases in the sediments can produce a similar effect).

12. DEEP WATER TRIALS

PUPPI was deployed on Discovery Cruise 141 (October-November 1983). Objectives for this cruise were to test the mechanical, electrical and acoustic systems in deep water. The only modifications to the instrument since the shallow water tests were: (a) four fins were attached to provide a critically-damped system, as shown in Figure 11; (b) nylon tubing was used instead of copper; (c) the instrument was completely bled before deployment. PUPPI was assembled vertically over the aft hatch with the probe extending down into the hold and the lead weights and the rest of the instrument were supported by a modified hatch cover.

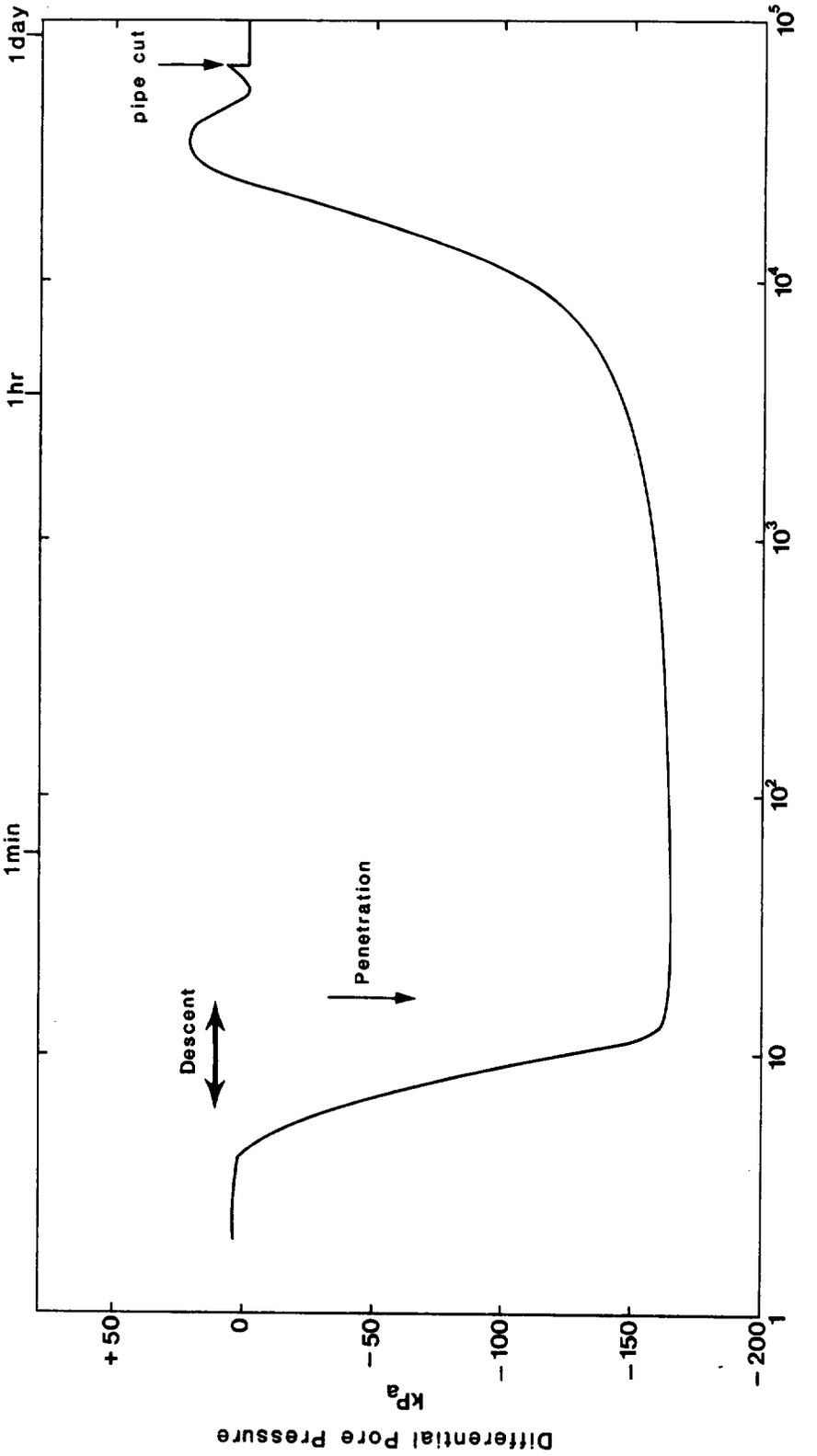

Figure 17: Differential pore pressure response for drop number 3 of the shallow water trials.

At Station No. 10943 (33°31.5'N, 22°58.05'W), PUPPI was launched using the crane and released by cutting the rope strop with a knife after an hydraulic cutter had failed to operate. It reached a terminal velocity of 2.5 ms^{-1} (with six lead weights attached) taking approximately 36 minutes to reach the bottom in 5407 metres of water. The acoustic telemetery indicated angles during descent and after penetration of less than 10°. The penetration rod was not pushed up after penetration (as indicated by a gated acoustic pulse) hence it was concluded that, while the instrument had not fully penetrated, it was close to vertical and stable in the seafloor. After 45 hours 35 minutes on the seafloor, the instrument was released by acoustic command and ascended at 0.76 ms^{-1}. Tilt pulses (up to 15°) indicated some oscillations of the device for a short period at around 400m above the seafloor. Apart from this, the instrument remained stable throughout the ascent. At the sea surface, the V.H.F. radio trasmitter proved valuable for locating the surfaced instrument. PUPPI was recovered using the stray line through the forward A-frame.

12.1 Accelerometer record

The accelerometer system behaved as designed and successfully recorded the penetration event. A ± 0.3 ms^{-2} noise level was recorded while the instrument was falling through the water column which is similar to that obtained during the shallow water trials. The deceleration profile is shown in Figure 18. After 0.6s the accelerometer overloaded (>1g) presumably because the instrument hit either a very stiff sediment layer or possibly even a rock. After this high deceleration, the resonance of the accelerometer prevented any further useful data being obtained. However, it is still possible to estimate the depth of penetration by double integrating this profile. The velocity and penetration profiles are also shown in Figure 18. A penetration depth of 1.4m is estimated from these profiles. The instrument has now been modified with a 5g accelerometer which has a higher resonant frequency (36 Hz). The velocity-penetration curve is shown in Figure 19. When compared with Figure 8 the upper 1.2 metres of sediment compares more closely with the stronger sediment modelled.

12.2 Pressure Record

A complete pressure record is shown from the time PUPPI was released to the time it was back on the sea surface in Figure 20. All pressures are calculated using the 'zero reference' value which is obtained immediately the pipe is cut at

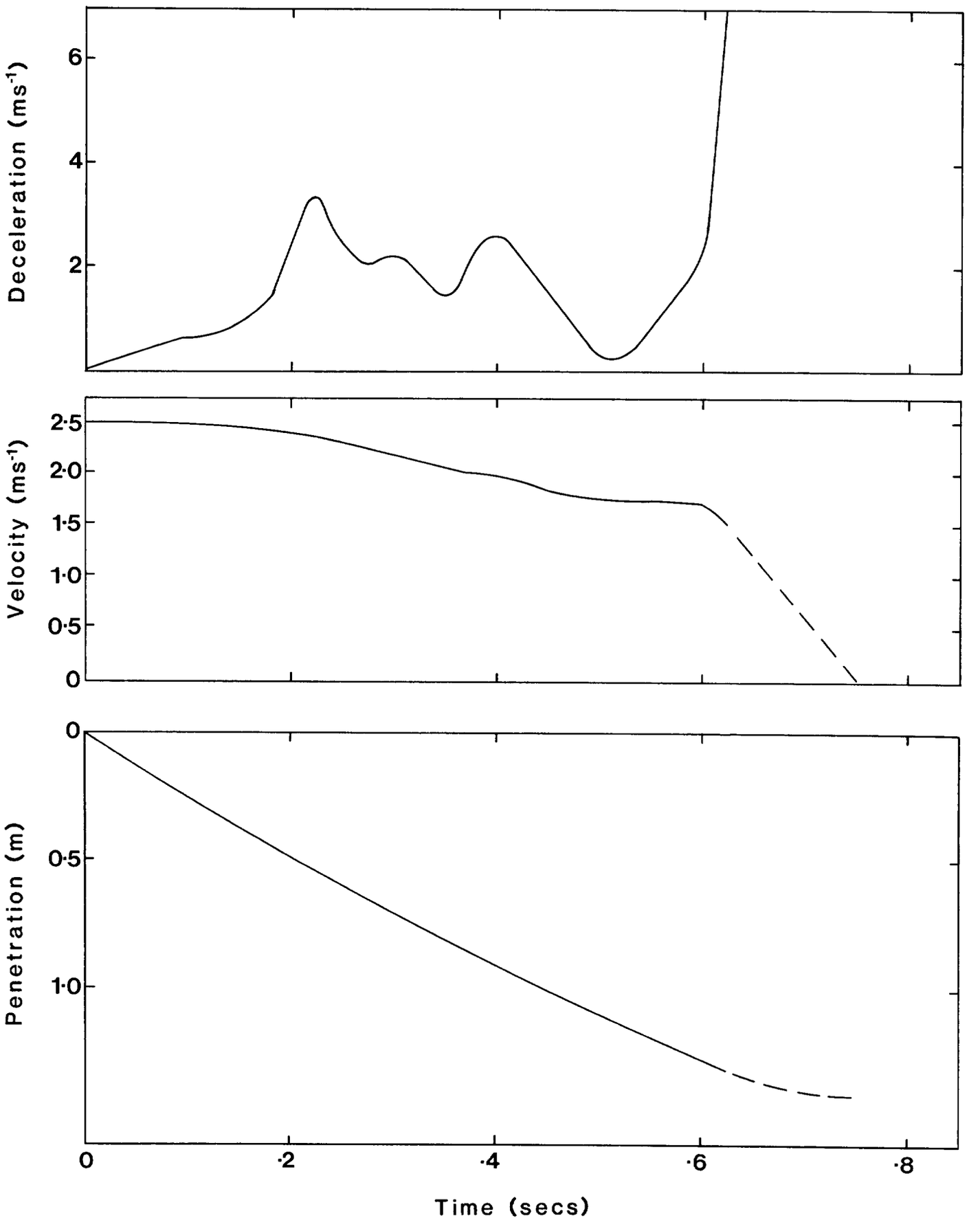

Figure 18: Deceleration, velocity and penetration curves for PUPPI station 10493.

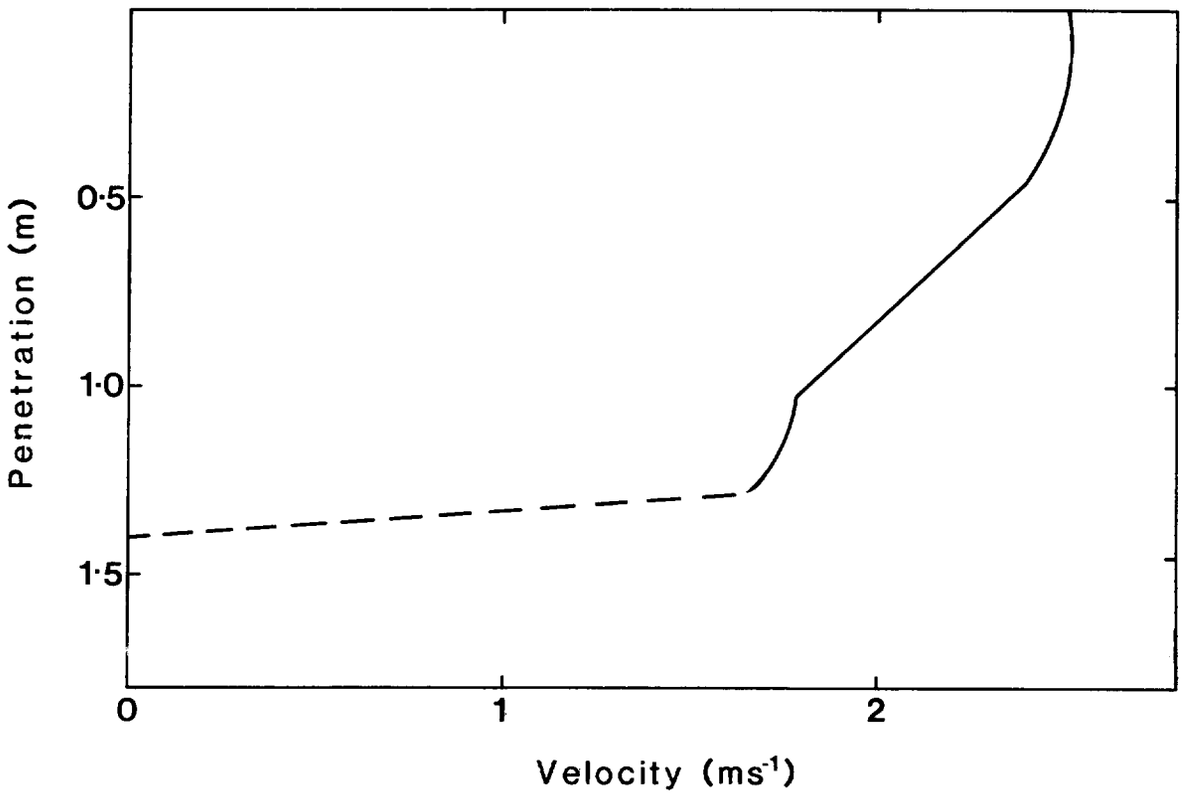

Figure 19: Velocity-penetration curve for PUPPI station 10493.

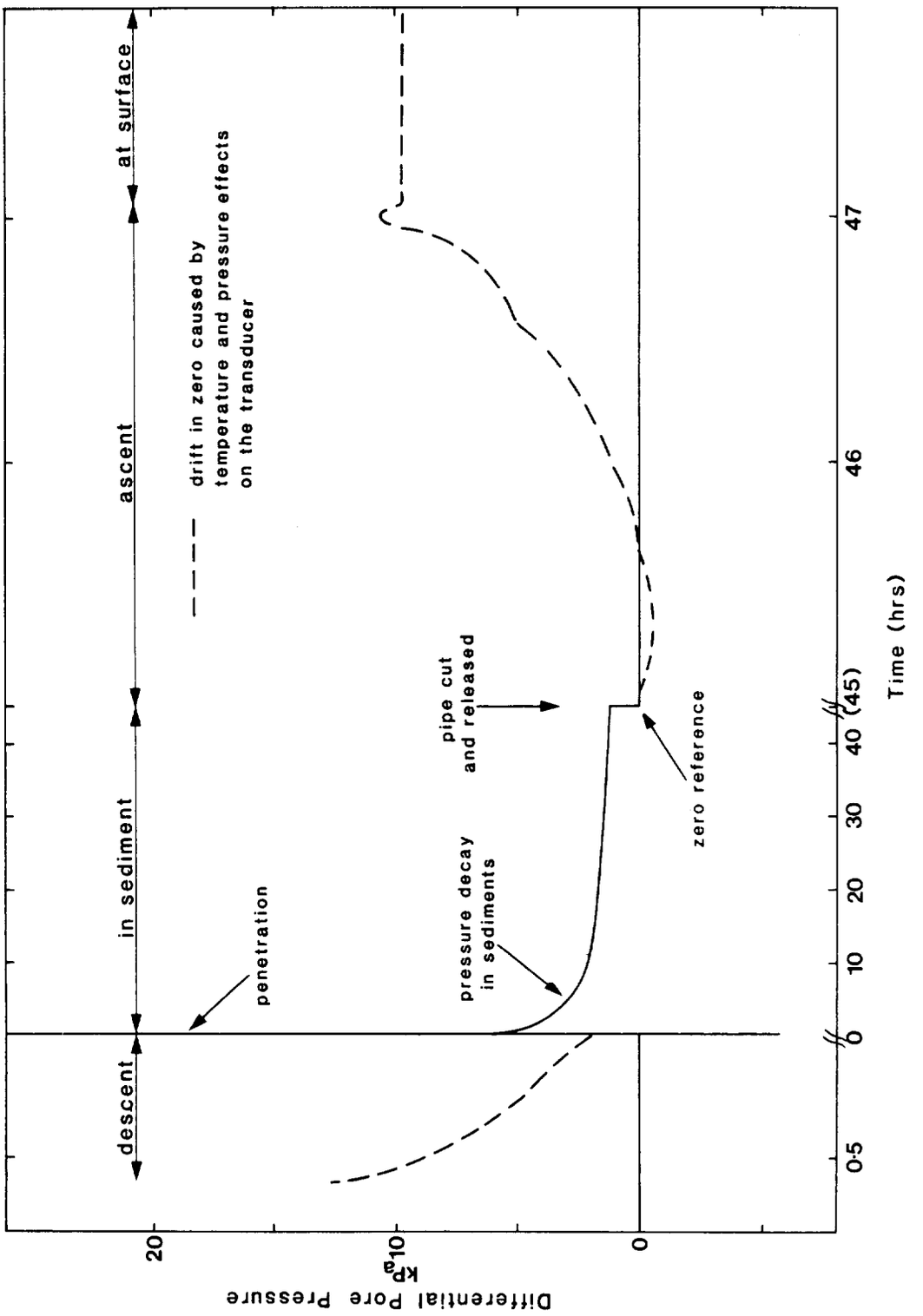

Figure 20: Differential pore pressure versus time for the complete deployment of PUPPI at station 10493.

the time of release from the sea floor. The dashed lines show the apparent pressure recorded during descent and ascent caused by a shift in the zero as a result of temperature and pressure effects on the transducer.

The penetration event and the subsequent decay of pore pressure is shown plotted against log time in Figure 21. A sharp discontinuity occurs at 25s which may have been caused by a small amount of settlement. A smoother discontinuity occurs at about one hour which reveals that two decay curves exist; one prior to one hour and one after one hour. This is more readily seen in Figure 22 where the pore pressure decay has been plotted against t^- . The two decay curves are represented on this plot as two straight lines with distinctly different gradients. Future deployments will enable this feature to be examined in more detail and its cause ascertained.

To estimate the pore pressure at time infinity, a straight line is drawn through the data and extrapolated to $t^- = 0, (t = \infty)$. This expanded and extrapolated section is shown in Figure 23. An extrapolated value of 0.28 kPa (= 0.028 m of water) is obtained which represents the true residual excess pore pressure. If the following values are used in equation 8, $k = 10^{-8}$ ms^{-1}, $n = 0.75$, $z = 1.4$m; then the advection velocity is 8 mm yr^{-1}.

At the same site, Noel (1983) reports two non-linear temperature profiles (from a total of six profiles, station 10405) one interpretation of which would indicate downward advection of pore water of 6.87 and 5.50 m/year. Not only does the magnitude of the results differ by three orders of magnitude but even the direction of flow is opposite.

13. FUTURE DEVELOPMENTS

The instrument as described in this report has functioned well for one deployment. It will require several more deployments before the reliability can be accurately assessed; these are currently scheduled to occur in October/November 1984. Apart from modification which may be needed as experience is gained from future deployments, there are two developments to this instrument which are currently being investigated.

1. Additional pore pressure ports (at different heights down the probe) and transducers to provide an accurate assessment of the variation in pore pressure gradient with depth.
2. The incorporation of a valve into the pore pressure line to enable the 'zero reference' pressure to be ascertained with more certainty. It is anticipated that this valve would be opened at some time prior to recovery

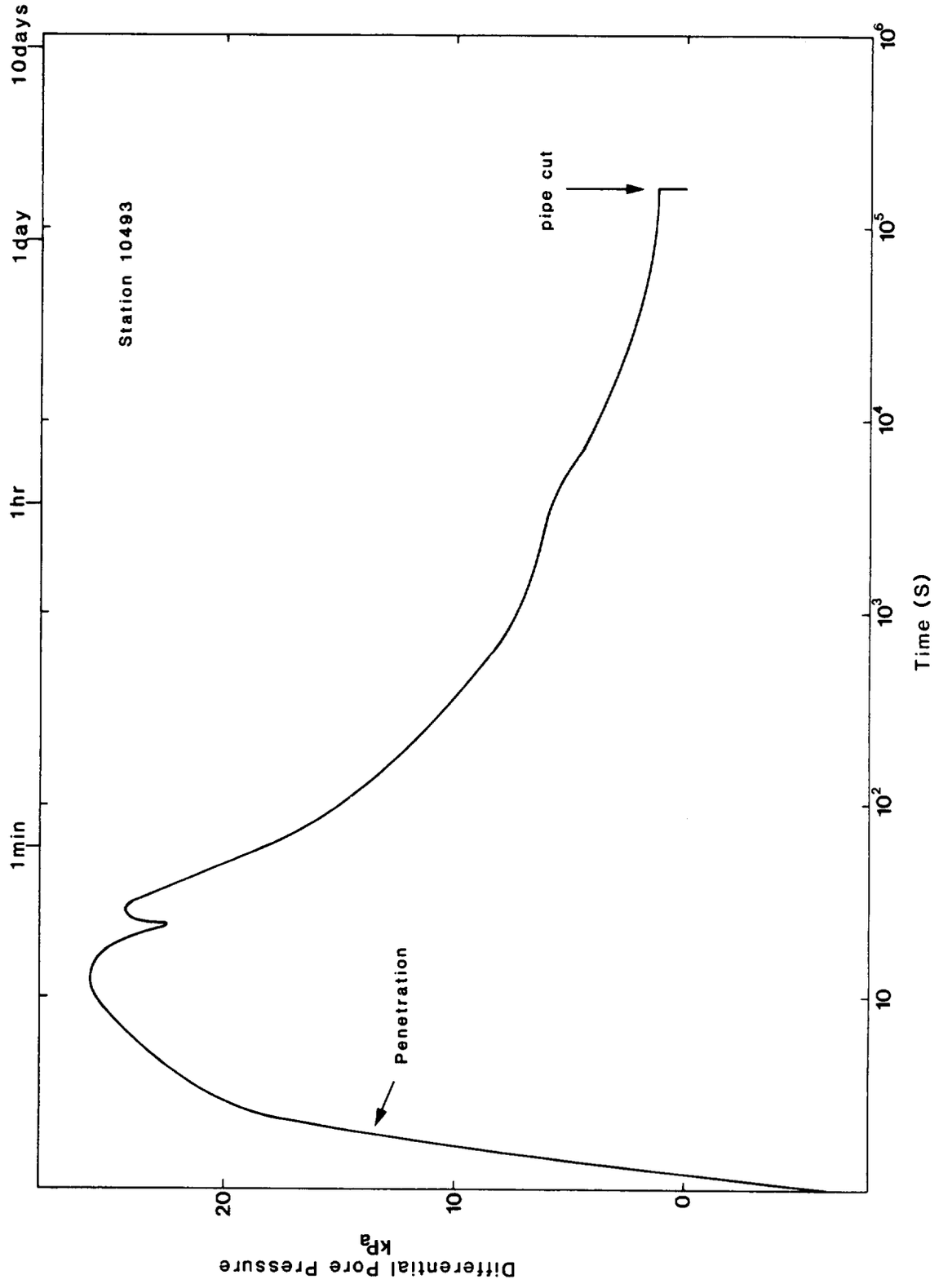

Figure 21: The pore pressure pulse and its decay.

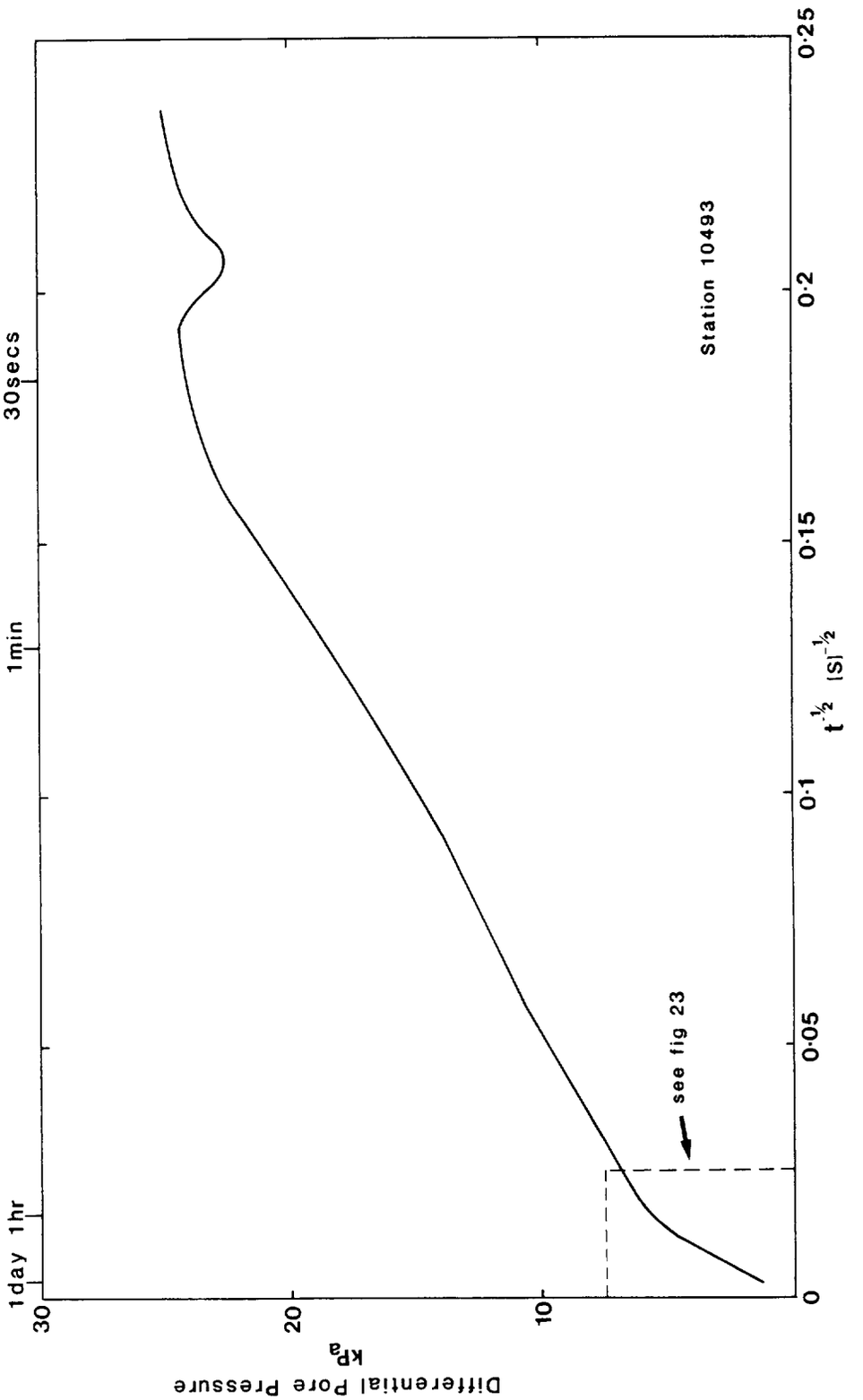

Figure 22: The decay of pore pressure versus $t^{-\frac{1}{2}}$.

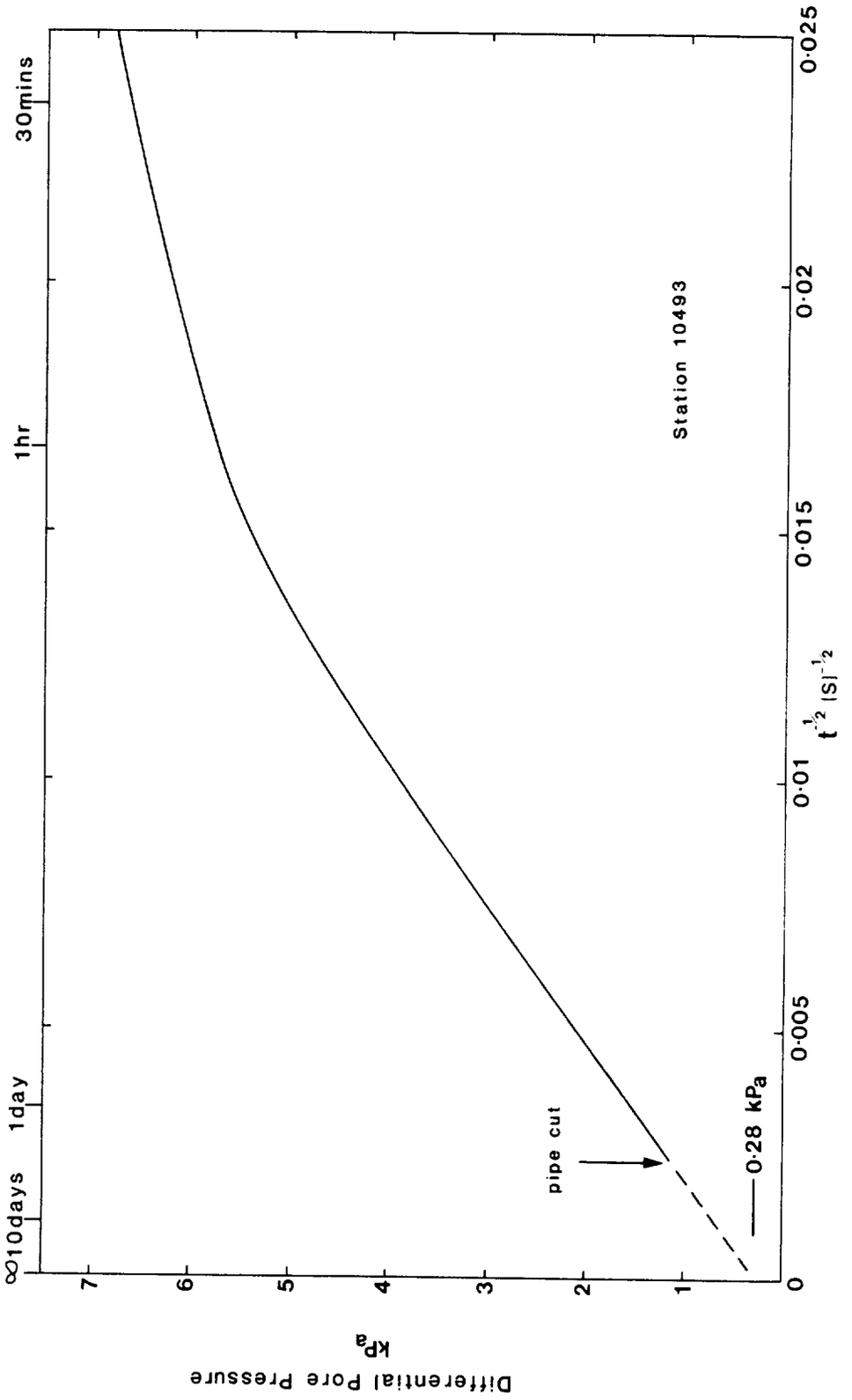

Figure 23: Extrapolation of the pore pressure decay to time infinity.

so that a large number of zero readings can be logged.

3. A variable speed flow pump if activated after the pore pressure had decayed sufficiently would enable the in-situ permeability to be assessed. A flow pump has been designed for use in the laboratory and it currently being assessed for use on PUPPI.

One of the major problems associated with pore pressure measurements of the kind described in this report is the length of time required to obtain the data. To map even a small area (say an area 10 km x 10 km) would perhaps require 100 deployments at a spacing of 1 km which would take an excessively long time with only one instrument. It would seem, therefore, that an array of these instruments (possibly 5-10) should be laid on the sea floor at any one time so that a sensible data rate can be achieved.

ACKNOWLEDGMENTS

We would like to thank R.B. Whitmarsh, T.J.G. Francis and G. Sills for reviewing this paper and for providing helpful comments. We also extend our thanks to the Director of the Scottish Marine Biological Association for enabling us to perform the shallow water trials using R.V. Calanus. Particular thanks go to A. Gale, G. Selby Smith and the crew of R.V. Calanus for their enthusiastic help during the trials.

REFERENCES

Abbott, D.H., Menke, W. and Morin, R., 1983. Constraints upon water advection in sediments of the Mariana Trough. J. Geophys. Res., 88, 1075-1093.

Anderson, R.N., Hobart, M.A. and Langseth, M.G., 1979. Geothermal convection through oceanic crust and sediments in the Indian Ocean. Science, 204, 828-832.

Anderson, R.N., Honnorez, J., Becker, K., Adamson, A.C., Alt, J.C., Emmerman, R., Kempton, P.D., Kinoshita, H., Laverne, C., Mottl, M.J. and Newmark, R.L., 1982. DSDP Hole 504B, the first reference section over 1 km through Layer 2 of the oceanic crust. Nature, 300, 589-594.

Becker, K. and Von Herzen, R.P., 1983. Heat flow on the western flank of the East Pacific Rise at 21°N. J. Geophys. Res., 88, 1057-1066.

Burgess, M. and Judge, A., 1981. Heat flow studies in the Sohm Abyssal Plain and their relevance to nuclear waste disposal investigations. Report to the Div. of Seismology and Geothermal Studies. Energy Mines and Resources, Canada.

Corliss, J.B., Dymond, J., Gordon, L.I., Edmond, J.M., Von Herzen, R.P., Ballard, R.D., Green, K., Williams, D.L., Bainbridge, A., Crane, K. and Van Andel, T.H., 1979. Submarine thermal springs on the Galapagos Rift. Science, 203, 1073-1083.

Crowe, J. and McDuff, R.E., 1979. Temperature and pore water chemistry profiles in the equatorial Pacific: incompatible results? EOS, Trans. AGU, 60, 863.

Dayal, U. and Allen, J.H., 1975. The effect of penetration rate on the strength of remoulded clay and sand samples. Canad. Geotech. J.., 12, 336-348.

Hinga, K.R., Heath, G.R., Anderson, D.R. and Hollister, C.D., 1982. Disposal of high-level radio-active wastes by burial in the seafloor. Environmental Science and Technology, 16, 1, 28A-37A.

Hoerner, S.F., 1958. Fluid dynamic drag. Published by author.

Klett, R.D., 1983. Pers. Comm.

Langseth, M.G. and Herman, B.M., 1981. Heat transfer in the oceanic crust of the Brazil Basin. J. Geophys. Res., 86, 10805-10819.

Litkouhi, S., 1979. The behaviour of foundation piles during driving. Ph. D. Thesis, London University.

Macdonald, K.C. and Luyendyk, B.P., 1981. The crest of the East Pacific Rise. Earth Planet. Sci. Lett., 48, 1-7.

Noel, M.J., 1983. Measurements of sediment temperatures, conductivity and heat flow in the North Atlantic and their relevance to radioactive waste disposal. IOS Report No. 172.

Noel, M.J., 1983a. Origins and significance of non-linear temperature profiles in deep-sea sediments. Geophys. J. R. astr. Soc. (in press).

Phillips, G.R.J., 1981. The IOS acoustic command and monitoring system: Part 3 - releases, beacons and transponders. IOS Report No. 96/3, unpublished manuscript.

RISE Project Group, 1980. Hot springs and geophysical experiments on the East Pacific Rise. Science, 207, 1421-1433.

Schultheiss, P.J. and Gunn, D.E., 1984. Consolidation and permeability of deep-sea sediments. IOS Report (in prep.)

Williams, D.L., Green, K., Van Andel, T.H., Von Herzen, R.P., Dymond, J.R. and Crane, K., 1979. The hydrothermal mounds of the Galapagos Rift: Observations with DSRV Alvin and detailed heat flow studies. J. Geophys. Res., 84, 7467-7484.